Journal of Nanobiotechnology

REVIEW

Open Access

Aggregation-induced emission photosensitizer-based photodynamic therapy in cancer: from chemical to clinical

Zijuan Meng[1], Huiying Xue[1], Tingting Wang[1], Biao Chen[3], Xiyuan Dong[3], Lili Yang[2*], Jun Dai[3*], Xiaoding Lou[1] and Fan Xia[1]

Abstract

Cancer remains a serious threat to human health owing to the lack of effective treatments. Photodynamic therapy (PDT) has emerged as a promising non-invasive cancer treatment that consists of three main elements: photosensitizers (PSs), light and oxygen. However, some traditional PSs are prone to aggregation-caused quenching (ACQ), leading to reduced reactive oxygen species (ROS) generation capacity. Aggregation-induced emission (AIE)-PSs, due to their distorted structure, suppress the strong molecular interactions, making them more photosensitive in the aggregated state instead. Activated by light, they can efficiently produce ROS and induce cell death. PS is one of the core factors of efficient PDT, so proceeding from the design and preparation of AIE-PSs, including how to manipulate the electron donor (D) and receptor (A) in the PSs configuration, introduce heavy atoms or metal complexes, design of Type I AIE-PSs, polymerization-enhanced photosensitization and nano-engineering approaches. Then, the preclinical experiments of AIE-PSs in treating different types of tumors, such as ovarian cancer, cervical cancer, lung cancer, breast cancer, and its great potential clinical applications are discussed. In addition, some perspectives on the further development of AIE-PSs are presented. This review hopes to stimulate the interest of researchers in different fields such as chemistry, materials science, biology, and medicine, and promote the clinical translation of AIE-PSs.

Keywords: Aggregation-induced emission, Photosensitizers, Photodynamic therapy, Cancer therapy, Clinical translation

*Correspondence: 695711363@qq.com; dj_hust1987@sina.com; jundai@tjh.tjmu.edu.cn

[2] Institute of Pathology, Tongji Hospital, Tongji Medical College, Huazhong University of Science and Technology, Wuhan 430034, China
[3] Department of Obstetrics and Gynecology, Tongji Hospital, Tongji Medical College, Huazhong University of Science and Technology, Wuhan 430034, China
Full list of author information is available at the end of the article

Graphical Abstract

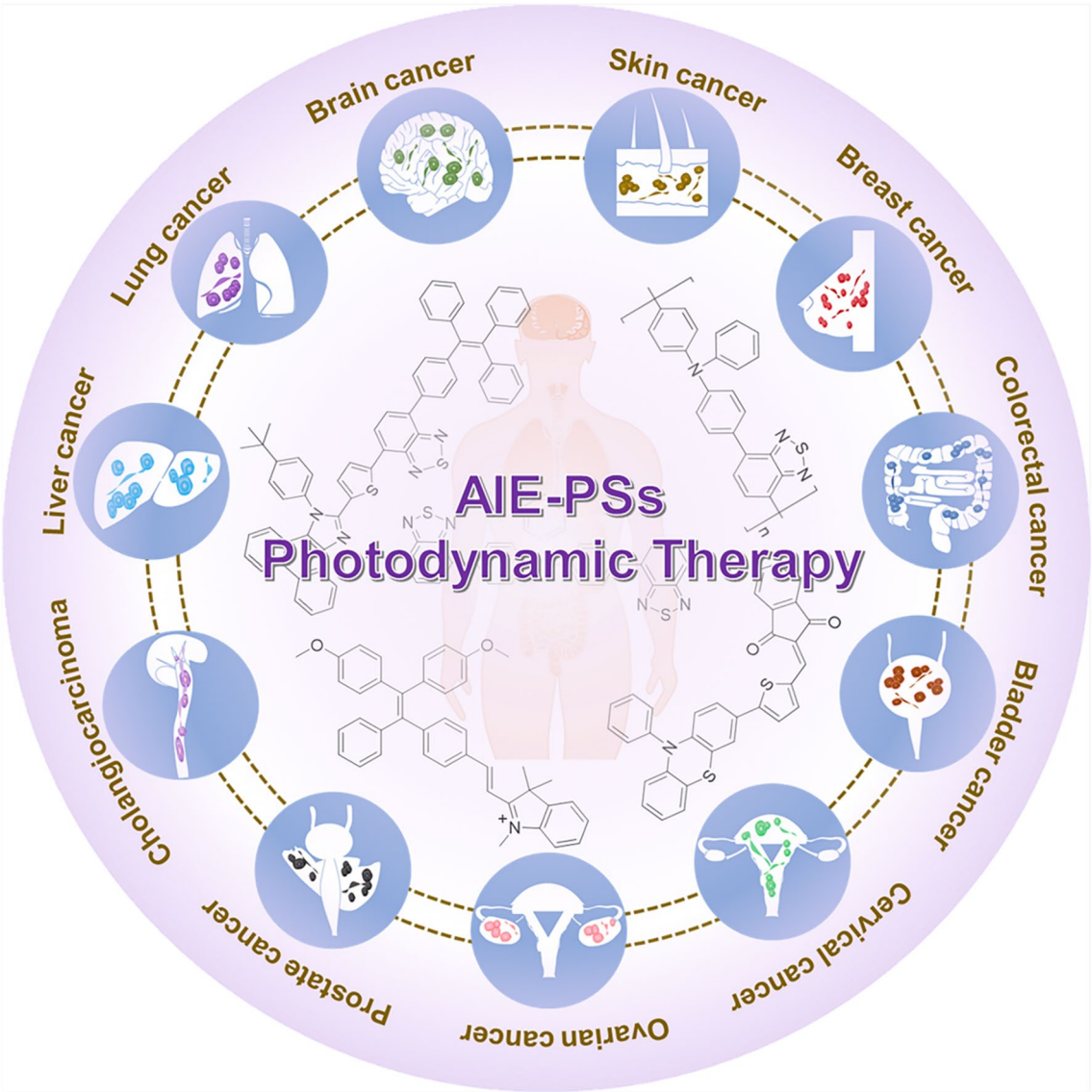

Background

The incidence and mortality rates of cancer are increasing rapidly in countries around the world [1, 2]. Cancer is a mortal disease that is relatively difficult to cure because of its uncontrollable and ultrafast proliferation properties [3, 4]. Thus, it is of profound significance for human health to explore highly effective and active therapeutic approaches for cancer. With the advent of PDT, approaches for treating tumors have been further expanded [5–8]. PDT has undergone a long period of development since the specific cytotoxic effects of combining acridine dyes with light to lead to tumor ablation were demonstrated in 1900 [9]. Due to its minimal invasiveness, high safety, in situ maneuverability and high spatiotemporal precision, it has eventually been used as a photo-regulated therapeutic modality for cancers and other diseases in clinical therapy [10–12]. Although PDT was the first drug-device combination authorized by the United States Food and Drug Administration (FDA), it is still not fully utilized in clinical practice [13, 14]. Therefore, improving the utilization rate and therapeutic ability of PDT is an urgent need to advance clinical tumor treatment.

During PDT, PSs are initiated by light irradiation at a specific wavelength, which matches the absorption of PSs, to produce ROS, primarily including $^1O_2$, $O^{2\bullet-}$, •OH and peroxides, to damage the pathological lesions [15]. However, the practical application shows that ROS has a short half-life (less than 40 ns) and a limited diffusion distance (up to 20 nm) in the organism, which is also a limitation that traditional PDT is not yet widely used for clinical tumor therapy [16]. So far, several PSs have been approved for clinical treatment of tumors, such as porfimer sodium (Photofrin) (HPD) [17], 5-aminolevulinic acid (ALA) [18], ALA esters [19], temoporfin (Foscan) (mTHPC) [20, 21] and verteporfin [22, 23]. Unfortunately, the photosensitivity of conventional PSs is severely impaired by ACQ and photobleaching, resulting in limited application in tumor therapy [24–27]. It was not until 2001 that Tang's research group discovered a phenomenon opposite to ACQ, which showed that the higher the degree of aggregation of fluorescent molecules, the stronger the fluorescence, and named this phenomenon as AIE [28]. In the aggregated state, the fluorescence emission of AIE luminogens (AIEgens) is enhanced, as is their ability to generate ROS [29]. These properties are the reasons why AIEgens are widely used in biomedical fields such as biomolecular labeling, organelle imaging, cell tracking, antibacterial agents and disease diagnosis [30–46], and even make them excellent candidates to be PSs for PDT [47–50]. AIEgens-based PSs were reported by Liu and Tang et al. in 2014, which have attracted extensive attention [51]. Almost the same time, Hu et al. developed a new red-emissive bioprobe, TPE-red-2AP2H, which was successfully used to track the intracellular motion of the lysosomal protein transmembrane 4 beta (LAPTM4B) protein. Even better, $^1O_2$ was generated under visible light, making this bioprobe potential for targeted photodynamic therapy as well [52]. In addition, novel therapeutic strategies that combine PDT with chemotherapy, photothermal therapy (PTT), immunotherapy or radiotherapy have been explored by researchers, so as to improve the efficacy of cancer treatment [53–59].

This review focuses on the recent studies of AIE-PSs in the treatment of various cancers. First, the principles and mechanisms of ROS generation are introduced, followed by the design and efficient manufacture of AIE-PSs. AIE-PSs-based PDT has been explored in preclinical trials for the treatment of tumors. Therefore, we summarize the potential of these AIE-PSs in cervical cancer, ovarian cancer, brain cancer, breast cancer, skin cancer, lung cancer, colorectal cancer, bladder cancer, colorectal cancer, bladder cancer and liver cancer from a clinical perspective. Meanwhile, we hope to promote the development of new anticancer strategies by exploring efficient PSs, including two-photon AIE-PSs and nano-functionalized AIE-PSs, to enable the application of AIE-PSs in clinical cancer therapy.

Design of AIE-PSs for PDT

PDT is driven by physical processes of light that occurs between the excited photosensitizer and the surrounding oxygen or biological substrate environment [60, 61]. Efficient ROS generation is a decisive factor in the effectiveness of PDT, so improving the efficiency of ROS generation is one of the key factors in the design of AIE-PSs. Through the Jablonski diagram, we can clearly explain the mechanism of molecular fluorescence emission and production of ROS, which provides corresponding theoretical support for the rational design of PSs [62, 63]. As shown in Fig. 1, once molecules are excited by photons from the ground state (S_0) to higher-energy orbitals (S_n), the excited molecules will release energy during the internal conversion (IC), returning to the lowest singlet excited state (S_1) [64]. There are three main pathways for S_1 excitation, among which fluorescence is generated when molecules return from S_1 to S_0 via radiative decay, which can be used in the field of fluorescence imaging. In addition to fluorescence emission, non-radiative decay back to S_0 also produces heat available for PTT. The final pathway is the transfer of S_1 to T_1 through intersystem crossover (ISC), in which electrons are transferred to the substrate to form toxic $O_2^{\bullet-}$, OH• and H_2O_2 for type I PDT, or transfer their energy to the surrounding oxygen to form $^1O_2$ at T_1 state for type II PDT. Therefore, for the PS molecules designed for PDT, the efficiency of ISC in reducing the energy gap between the excited S_1 and T_1 states (ΔE_{ST}) is the most critical factor.

The AIE phenomenon is mainly based on the mechanism of restricted intermolecular motion (RIM) [65–67]. When the molecules are in the aggregated state, the IC is prevented by restricted intramolecular motions, resulting in excited molecules to T_1 through the radiative transition or ISC. PSs in the T_1 state can undergo a series of reactions with surrounding substrates, thereby promoting the production of various ROS. The AIE-PSs generally enjoy promoted radiative pathways with suppressed non-radiative decay pathway in aggregation, leading to the production of more ROS, which has the potential to become the dominant molecule in PDT. Figure 2 summarizes the molecular structures of AIE PSs involved in this section.

Manipulation of electron donor (D) and acceptor (A)

According to the above theoretical basis, we can know that ISC can be facilitated by reducing the ΔE_{ST} of the PSs to increase the generation of ROS [68]. Therefore, minimizing ΔE_{ST} is one of the key factors to achieve high

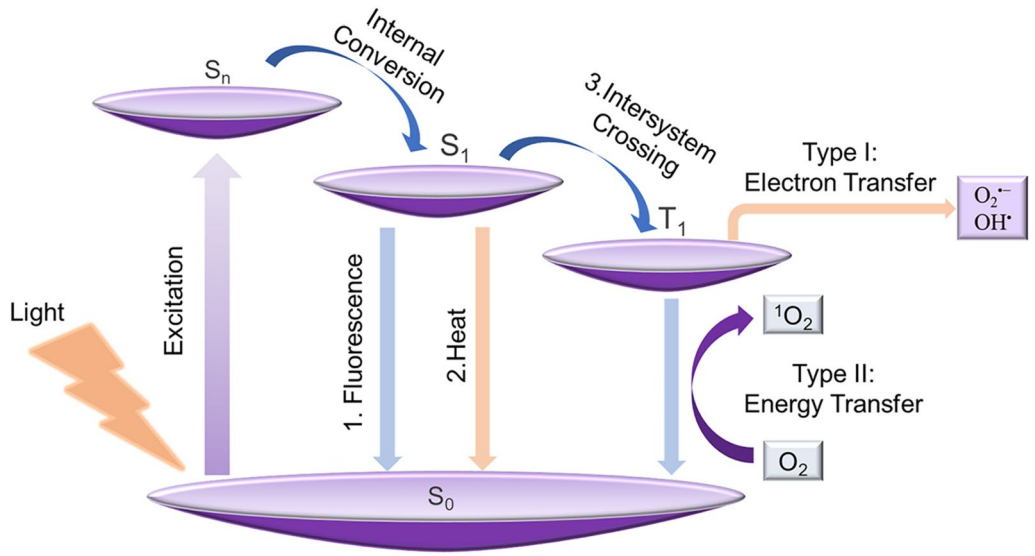

Fig. 1 A Jablonski diagram explaining the working mechanism of type I and type II PSs

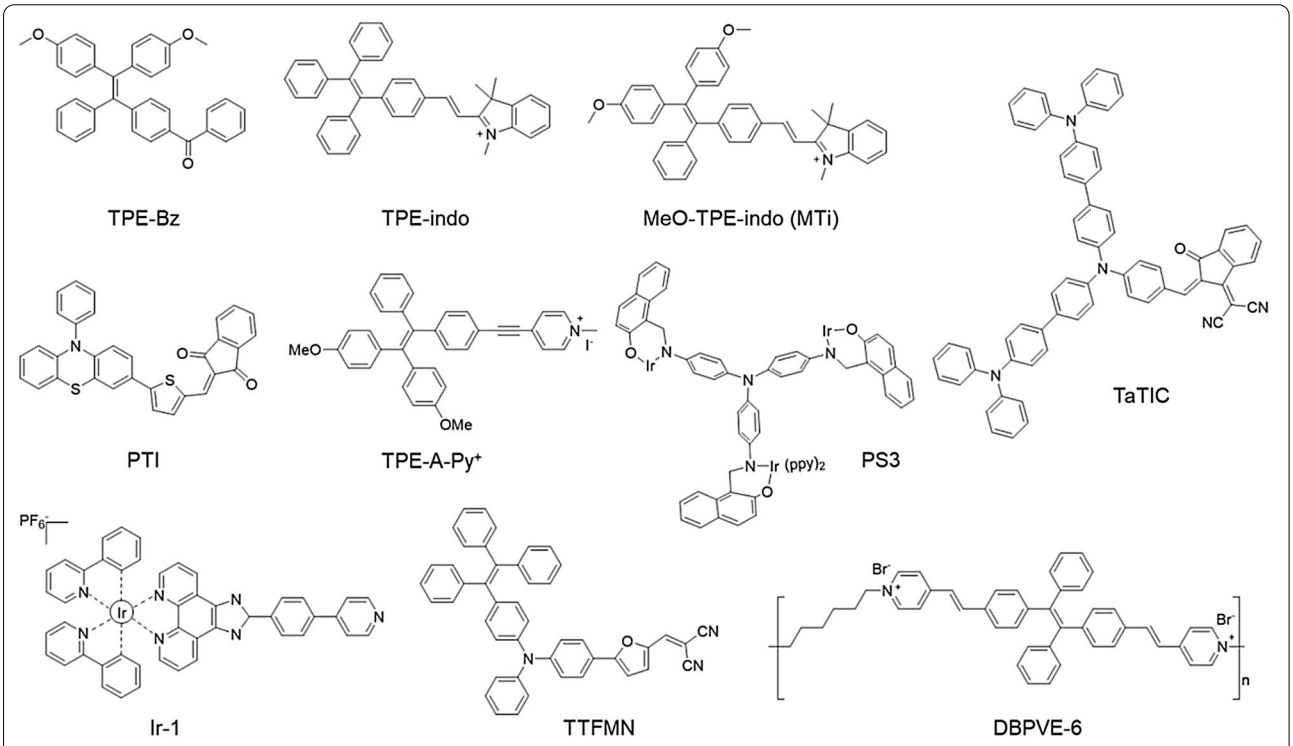

Fig. 2 The molecular structures of AIE-PSs summarized in this review

ROS production efficiency. The most commonly used molecular design strategy is to manipulate the connection between the D and A to reduce the overlap between the distributions of the highest occupied molecular orbital (HOMO) and the lowest unoccupied molecular orbital (LUMO). Wang's group designed a series of AIEgens based on tetraphenylethylene (TPE) skeletons to reduce ΔE_{ST}, and the results of theoretical calculations and experiments are sufficient to prove the feasibility of this strategy [69]. They introduced methoxyl and positively charged indole groups on a TPE skeleton, with the methoxyl as D and positively charged indole acts as

A group, to obtain the lowest ΔE_{ST} value. Compared to other molecules, the ΔE_{ST} of MTi is 0.633 eV, which is the lowest value among all molecules. This is an advantage of the molecule based on the D-A structure of methoxy and indole groups. Under the same white light irradiation (420–780 nm, 100 mW cm^{-2}, 3 min), the rate of $^1O_2$ generation was MTi > TPE-indo > TPE-BZ. The results indicated that the $^1O_2$ generation among these AIEgens was consistent with the change trend of ΔE_{ST} values. To obtain AIE-PSs with high $^1O_2$ efficiency, strong absorption and long wavelength emission, Lu et al. proposed a new molecular design strategy. The molecular design was started from TPT to achieve HOMO–LUMO separation for $^1O_2$ generation. Subsequently, a new AIE-PS named TBT was designed using different A, 2,1,3-benzothiadiazole (BT) and 2-dicyanomethylene-3-cyano-4,5,5-trimethyl-2,5-dihydrofuran (TCF), linked together by a double bond as the combined A and further linked to the methoxy substituted TPE D. As the combined A of TBT shows a stronger electron withdrawing capacity than the single A, the charge transfer in TBT is stronger than that in TPT, achieving smaller ΔE_{ST} value and the goal of high efficiency of $^1O_2$ generation [50]. So far, most of the reported AIE-PSs have been designed on the basis of this strategy, showing excellent ROS performances [70–76].

In addition, Tang et al. added different amounts of carbonyl groups (C=O) and cyanide groups (–CN) to the PSs design, in which the cyanide group is a strong electron acceptor, and the carbonyl group has a high spin–orbit coupling (SOC) effect due to its hybrid singlet and triplet transition electron configurations including n and π orbitals, thus resulting in decreased ΔE_{ST} value and increased SOC interaction [77]. Finally, these groups are bonded to the triphenylamine (TPA) electron donor via a small π bridge to obtain a series of triphenylamine-indole derivatives. To further enhance the electron D-A strength of the molecule, TPA was further modified by a series of electron donors to prepare a new molecule named TaTIC. The results confirmed that TaTIC achieved the highest ROS production ability compared with other synthesized molecules, even 2.42 times that of Rose Bengal (RB, a commercial PS). Therefore, their findings provided a new guidance for designing D-A type PSs to enhance photosensitization ability.

Introduction of heavy atom or metal complex

In the past few decades, researchers have extensively exploited the indraught of heavy atoms (such as iodine and bromine) into the molecular structures to develop AIE-PSs with high-efficiency ROS. This is because heavy atoms can promote ISC process between the S_1 and T_1 states. Currently, three methods are existed for introducing heavy atoms, one of which is to introduce halogen atom via covalent bond. For example, Tang's group synthesized an AIE-active model PS (PI) with good ROS production efficiency and NIR emission capability [78]. To enhance the ISC process, a thiophene ring was inlet into the backbone of PI by the heavy atom effect to obtain PTI. The H2DCFH-DA probe is commonly utilized to assess the efficiency of ROS generation. Compared to PI, the fluorescence intensity of H2DCFH-DA rose rapidly to nearly 80-fold that of PTI (30-fold). This confirmed that the indraught of heavy atoms can indeed improve the production efficiency of ROS. The remaining two methods are the formation of the ionic bonds (e.g., TPE-A-Py^+ [79]) and conjugated metal complexes with different ligands (e.g., PS3 [80], Ir-1 [81]). Unfortunately, the indraught of heavy atoms can lead to high dark toxicity, limiting their widespread applications.

Design of type I AIE-PSs

The majority of organic PSs have been reported to induce ROS via the Type II pathway, however, the production of $^1O_2$ through the Type II pathway is highly relying on the presence of oxygen, which limits its effectiveness in severely hypoxic solid tumors [82]. The Type I process mainly generates low O_2-dependent radical species, such as $O_2^{\bullet-}$ and $OH^{\bullet}$, therefore, the design of Type I PSs becomes a key requirement for PDT. To address this challenge, Kang et al. designed the compound TTFMN with typical D-A structure [83]. Remarkably, the extreme electronic defects of the two cyano units on TTFMN are expected to favor the generation of Type-I ROS. Different ROS indexes were used to further determine the types of ROS generated by TTFMN. It was found that TTFMN showed the strongest signal strength for hydroxyphenyl fluoresce (the •OH generation indicator), while ABDA or SOSG ($^1O_2$ indicator) had almost no apparent signal change, manifesting its best generation ability of •OH. In addition, as shown in Fig. 3, Zhuang et al. reported another approach for Type-I PSs, obtaining phosphine oxide-based isomers α-TPA-PIO and β-TPA-PIO with efficient generation capacities of Type I ROS [84]. Not only that, they further collaborated to develop a series of tailored PSs with strong electron-withdrawing ability based on 9,10-phenanthrenequinone (PQ) [85]. The highly efficient generation of Type I ROS and excellent photothermal conversion ability are resourcefully integrated into these PQ-cored PSs to achieve Type I photodynamic and photothermal combined antitumor treatment. Other detailed studies on the photophysical and photochemical mechanisms of AIE-PSs provided a reference for the molecular design of AIE-PSs basing on the Type I mechanism [86–89].

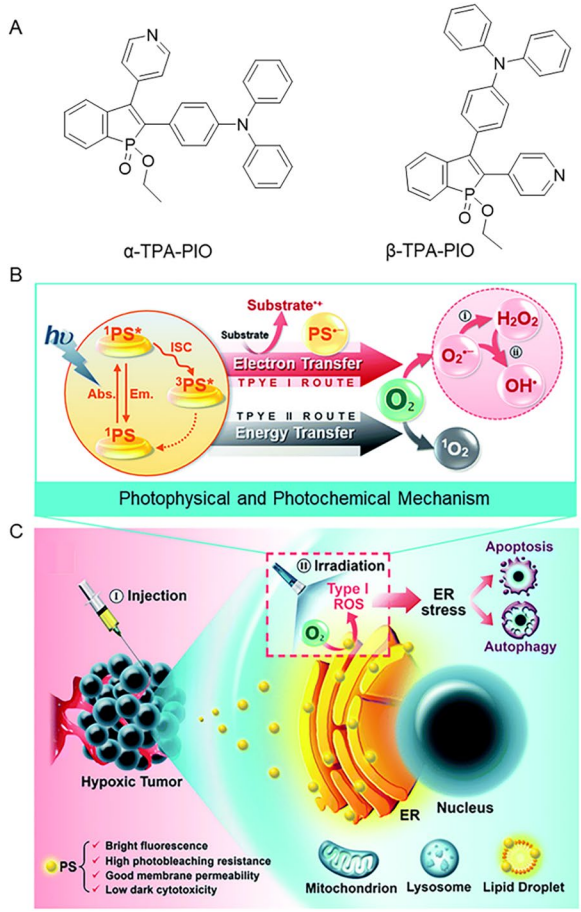

Fig. 3 **A** The construction of α-TPA-PIO and β-TPA-PIO. **B** The schematic diagram of the photophysical and photochemical mechanisms. **C** The cytological process of PDT therapy mediated via PIO-based fluorescein. Reprinted with permission [84]. Copyright 2020, Royal Society of Chemistry

Polymerization-enhanced photosensitization

For the past few years, AIE molecules have also been introduced into polymers. Especially compared with PSs based on organic small molecules, AIE polymers possess prominent advantages such as signal amplification effect, multiple functionalization, as well as good processability, etc. [25, 90, 91]. The general strategy for preparing AIE polymers is to add AIEgens into the framework or as side chains of the polymer by modification and polymerization [92]. Excitingly, Liu et al. confirmed that conjugated polymers exhibited higher generation efficiency of $^1O_2$ than their small-molecular counterparts (Fig. 4) [93]. By improving the strength of the conjugation, Zhu et al. synthesized four polyelectrolyte PSs with AIE fluorescence units, cationic units, conjugated units and aliphatic chains [94]. The ROS yields of DBPVE-6 under white light irradiation (400–700 nm, 60mW cm^{-2}) were the highest, which may be due to its long aliphatic chain. This inspired us to design PSs by changing the conjugation strength and aliphatic chain length to achieve regulation of photocatalytic efficiency.

Nano-engineering approaches

High ROS production could be guaranteed by molecular design to facilitate the ISC processes, but high ISC efficiency does not guarantee high ROS production in practical applications. Various inevitable problems will occur, such as poor solubility or destruction by polar solvents, when PSs are dispersed in the aquatic biological buffer. The preparation of nanoparticles is not only a simple method to overcome the hydrophobicity and biocompatibility problems of PSs, but also one of the strategies to improve ROS production. The long-life triplet states of nanoaggregates help to utilize the energy dissipation from S_1 to T_1 state, which is consistent with the principle of aggregation-induced ISC (AI-ISC). As shown in Fig. 5, Liu et al. synthesized NS-STPA by rigid coplanar grafting of flexible rotors and prepared them into nanoparticles (NS-STPA NPs), demonstrating that this method is an engineering approach to further improve ROS generation [95]. The apparent lifetime τ_T of triplet NS-STPA was 57.97 μs in DMSO, while its τ_T in nanoparticles was extended to 209.4 μs. Meanwhile, the ROS generation of NS-STPA and NS-STPA NPs was compared under the same conditions. The results indicated that the ROS generation property of NS-STPA NPs was significantly better than that of NS-STPA within a short irradiation time. These results demonstrated that the nanoengineered pathways had the ability to further enhance ROS production, which provided conditions for the clinical application of PSs. More encouragingly, the coated NPs can be modified on their surface by functional groups such as peptides, folic acid (FA), antibodies and membranes to obtain the desired bioactive functions [96–103], which would better satisfy the different clinical needs.

In addition, in order to improve the performance of PSs and reveal the possibility of its clinical application, the multi-functional modified AIE-PSs had also been extensively studied. The hydrophobicity of most AIEgens hinders their application in organisms, and using of polymer encapsulation is one of the strategies to overcome this problem. Polyethylene glycol (PEG) is a nontoxic polymer with good biocompatibility and excellent drug encapsulation efficiency [104, 105]. It avoids the removal of the reticuloendothelial system during in vivo circulation, resulting in reduced immunogenicity, which makes PEG the most commonly used polymer material for the preparation of nanoparticles (NPs). Meanwhile, Pluronic F127 is a highly biocompatible amphiphilic block copolymer that is commonly used as a coating for

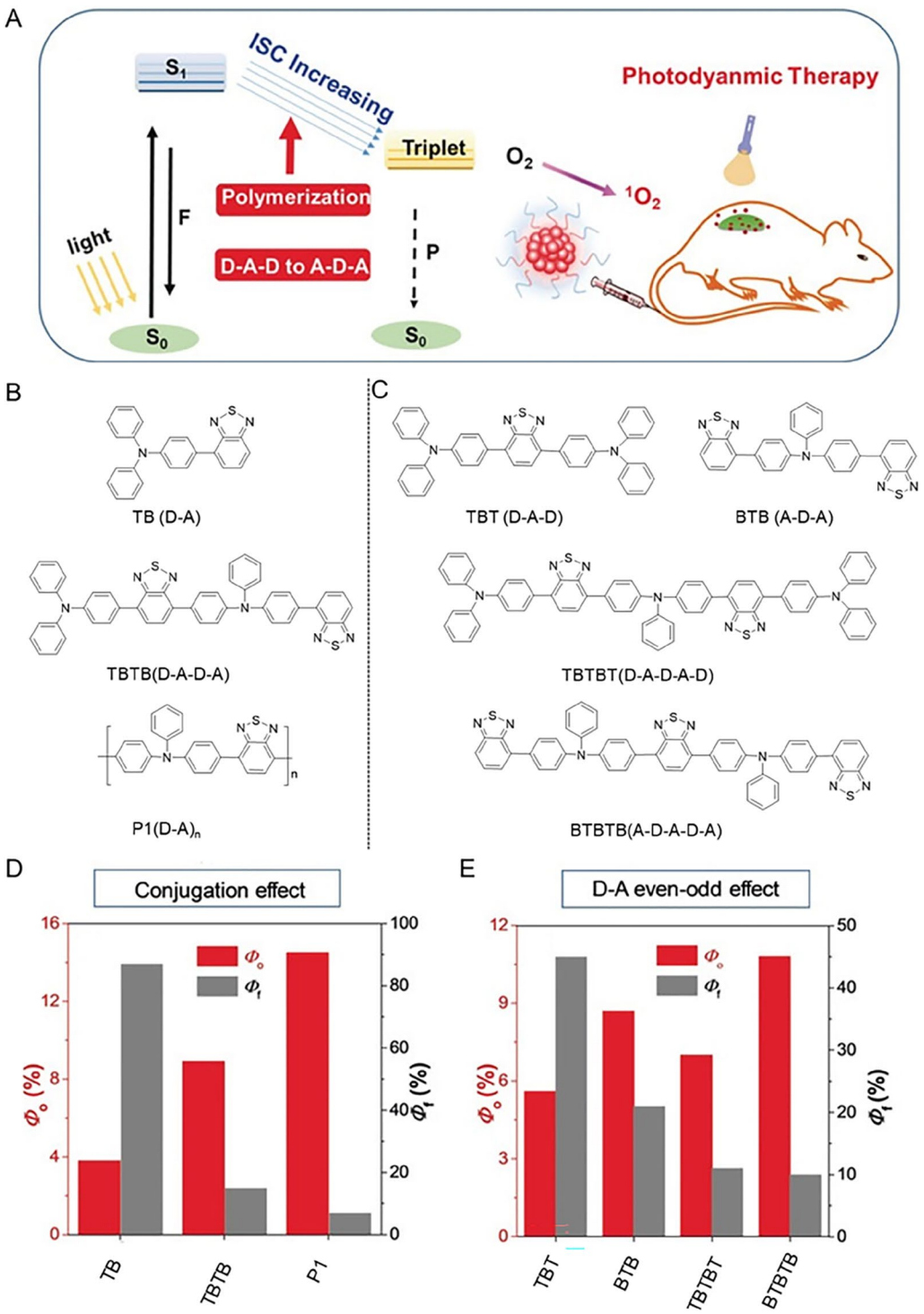

Fig. 4 **A** Enhanced photosensitization for application in PDT. **B** Chemical structures of TB, TBTB and P1. **C** Chemical structures of TBT, BTB, TBTBT and BTBTB. **D** and **E** $^1O_2$ quantum yield (Φ_o) and fluorescence quantum yield (Φ_F) of materials. Reproduced with permission [93]. Copyright 2018, Wiley–VCH

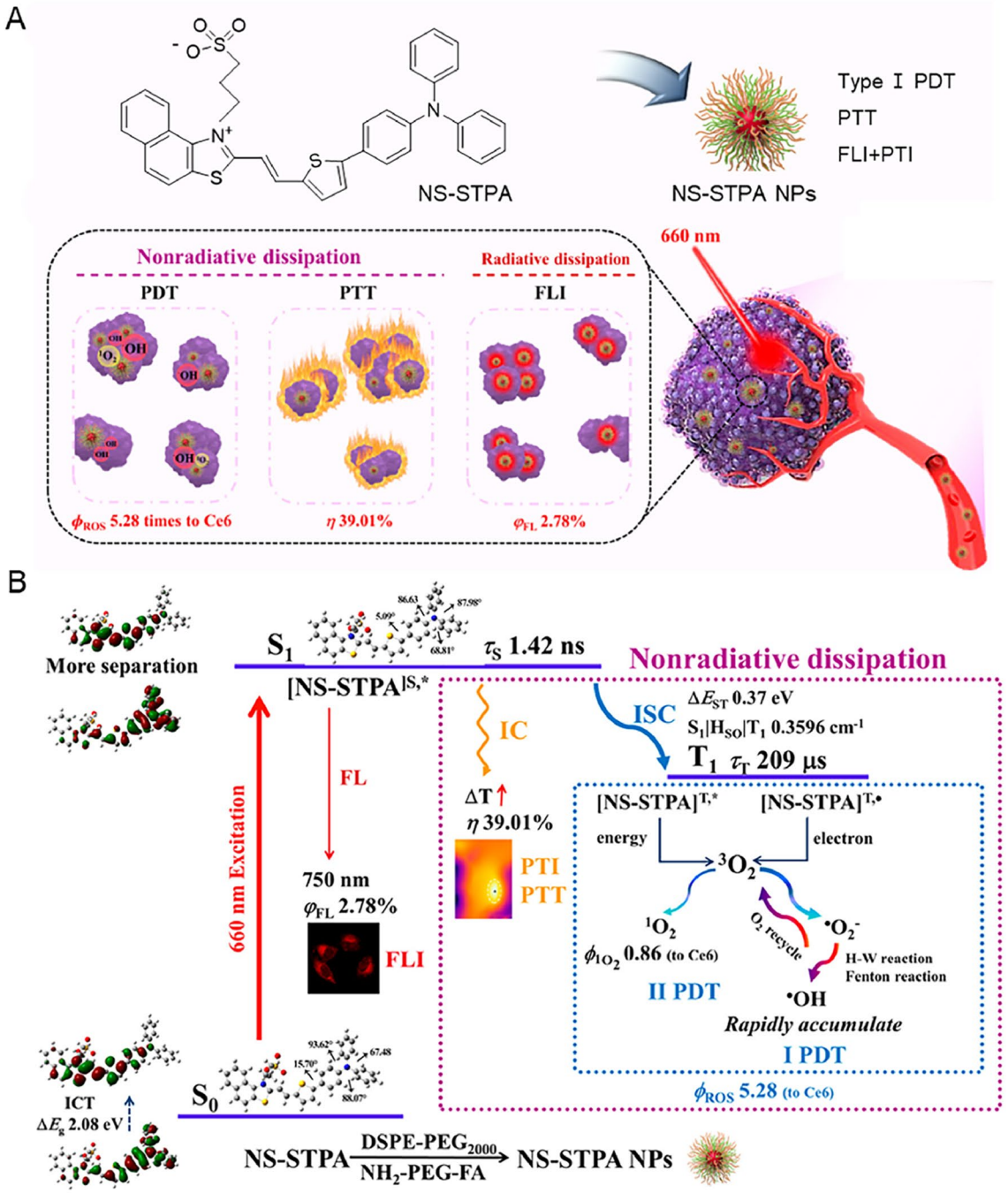

Fig. 5 **A** The construction of NS-STPA and scheme of the application of NS-STPA NPs in fluorescence imaging-guided multimodal phototherapy. **B** The excited-state dissipation mechanism of NS-STPA NPs illustrated by the simplified Jablonski diagram. Reproduced with permission [95]. Copyright 2022, American Chemical Society

the preparation of nanoparticles [106]. To achieve the purpose of local aggregation of AIE-PSs in tumor, both targeted peptides (*e.g.* RGD peptide [107, 108]) and penetrating peptides (*e.g.* TAT peptide [109, 110]) contribute their own advantages to this end.

AIE-PSs for different cancers treatment

Ovarian cancer

Ovarian cancer has the highest mortality rate among gynecological malignancies, and the current treatment is surgery combined with chemotherapy regimen of

paclitaxel/carboplatin [111]. At the beginning of treatment, most patients can effectively relieve, but the five-year survival rate is still less than 40% [112]. The main reasons are the high metastasis and high recurrence rates after treatment [113]. PDT effectively prolongs the survival of patients who cannot receive surgery, which has caused great concern. Tayyaba Hasan et al. have developed a photo-immune-regulating-liposome (PICAL), using an FDA-approved photosensitizer called Benzoporphyrin acid A (BPD) and an Cetuximab antibody for epidermal growth factor receptor (EGFR) to from Preformed Plain Liposome (PPL) [114]. The results showed that PPL increased the mortality of ovarian cancer cells. However, because of its low tissue penetration, these drugs can improve skin photosensitivity, reduce tumor specificity, lead to low human drug-resistant dose and tumor killing, so new photosensitizer is urgently needed to solve these problems.

AIE molecules are used for photodynamic treatment and image guidance, and have the advantages of avoiding the weak fluorescent signal caused by the ACQ effect. In order to further reduce background fluorescence interference and strong tissue penetration, an fluorogen including an electron-accepting benzo[1,2-b:4,5-b′] dithiophene 1,1,5,5-tetraoxide core and electron-donating 4,4′-(2,2-diphenylethene-1,1-diyl)bis(N,N-diphenylaniline) groups are used for PDT therapy and imaging, named TTB. Meanwhile, integrin $\alpha_v\beta_3$ has been reported to be an extremely important biomarker overexpressed in primary ovarian cancer cells, which has become a basis for the preparation of materials targeting ovarian cancer. Based on this, Dai and Li et al. simply encapsulated TTB into a biocompatible and water-soluble polymer matrix, 1,2-distearoyl-sn-glycero-3-phosphoethanolamine-N-[maleimide(polyethylene glycol)-2000] (MPD), in order to obtain good water-dispersible NPs [115]. To enhance the targeting ability of NPs to ovarian cancer cells, Mal-modified MPD/TTB NPs were prepared. Conjugation of MPD/TTB NPs to RGD peptide via the click reaction of SH and Mal groups resulted in RGD-MPD/TTB NPs that targeted the overexpressed integrin $\alpha_v\beta_3$ in ovarian cancer cells. Furthermore, an RGD-based modular peptide Arg-Gly-Asp-Phe-Gly-Gly-Arg-Arg-Arg-Arg-Cys (RGD-4R) carrying four arginine (R) was further designed. The RGD-4R peptide was grafted to MPD/TTB NPs through click reaction, which enhanced the ability of NPs to penetrate the cell membrane and facilitated the rapid entry of NPs into cells. The DCF signals were sequentially increased in SKOV-3 cells treated with MPD/TTB NPs, RGD-MPD/TTB NPs and RGD-4R-MPD/TTB NPs, while there was no significant difference in MCF7 cells (low expression of integrin $\alpha_v\beta_3$), suggesting that the ROS production efficiency of RGD-4R-MPD/TTB NPs was higher in SKOV-3 cells with overexpressed integrin expressing $\alpha_v\beta_3$ (Fig. 6). Finally, the ovarian cancer xenograft tumor model was established with SKOV-3 cells, and treatment was performed when the tumor volume reached 50 mm^3. The tumors in the RGD-4R-MPD/TTB NPs (light +) groups were significantly inhibited, and H&E staining, TUNEL staining and IHC staining of the tumor tissues confirmed that the PDT based on RGD-4R-MPD/TTB NPs had good biocompatibility and could effectively suppress the growth of ovarian cancer. More noteworthy, RGD-4R-MPD/TTB NPs showed good therapeutic effects on integrin $\alpha_v\beta_3$-overexpressed cervical cancer (HeLa cells) and prostate cancer (PC3 cells). To reduce the recurrence in ovarian cancer patients, Dai designed a modular peptide probe (T_{CD}TMP) comprising an AIE molecule (PyTPA) that can produce ROS efficiently [116]. It can self-assemble into NPs by loading miR-145-5p or VEGF-siRNA. This system reduces the recurrence rate of ovarian cancer in subcutaneous tumor models, abdominal metastasis models, and patient-derived tumor xenograft models, providing a new view for the surgical treatment of ovarian cancer.

To enhance tissue penetration, Wang et al. reported a two-photon cyclometalated iridium (III) complexes (Ir) fluorescent probe and further encapsulated into biocompatible NPs with a penetration depth of 300 μm [81]. At the same time, it also possesses high photoinduced ROS generation efficiency, and mitochondrial targeting ability, which can interfere with redox homeostasis in vitro, leading to mitochondrial dysfunction and cell apoptosis. This is because intrinsic pathway apoptosis is the most common cell death discussed within the context of PDT, so the research on mitochondrial activity is particularly prominent [117]. The tumor volume of 100 mm^3 of SKOV-3 tumor-bearing nude mice was treated with Ir-nanoparticles, and half of the nude mice tumors disappeared, whereas the tumor volume increased 26.2-folds in the PBS group. This provides a promising strategy for visualizing PDT therapy for ovarian cancer. The hypoxic environment at the tumor site greatly inhibits the therapeutic effect of PDT, so this article reports that the type I pathway PDT process. Not only that, the role of endoplasmic reticulum (ER) in PDT is not to be ignored. Immunogenic cell death (ICD) elicited by PDT is mediated through generation of ROS that induce ER stress [118]. The design of PSs for selective localization of the ER is the primary factor to determine the efficiency of PDT-induced ICD. Tang et al. constructed a PIO-based fluorophore that elicited ER stress and a dual cell death consisting of autophagy and apoptosis in vivo [84].

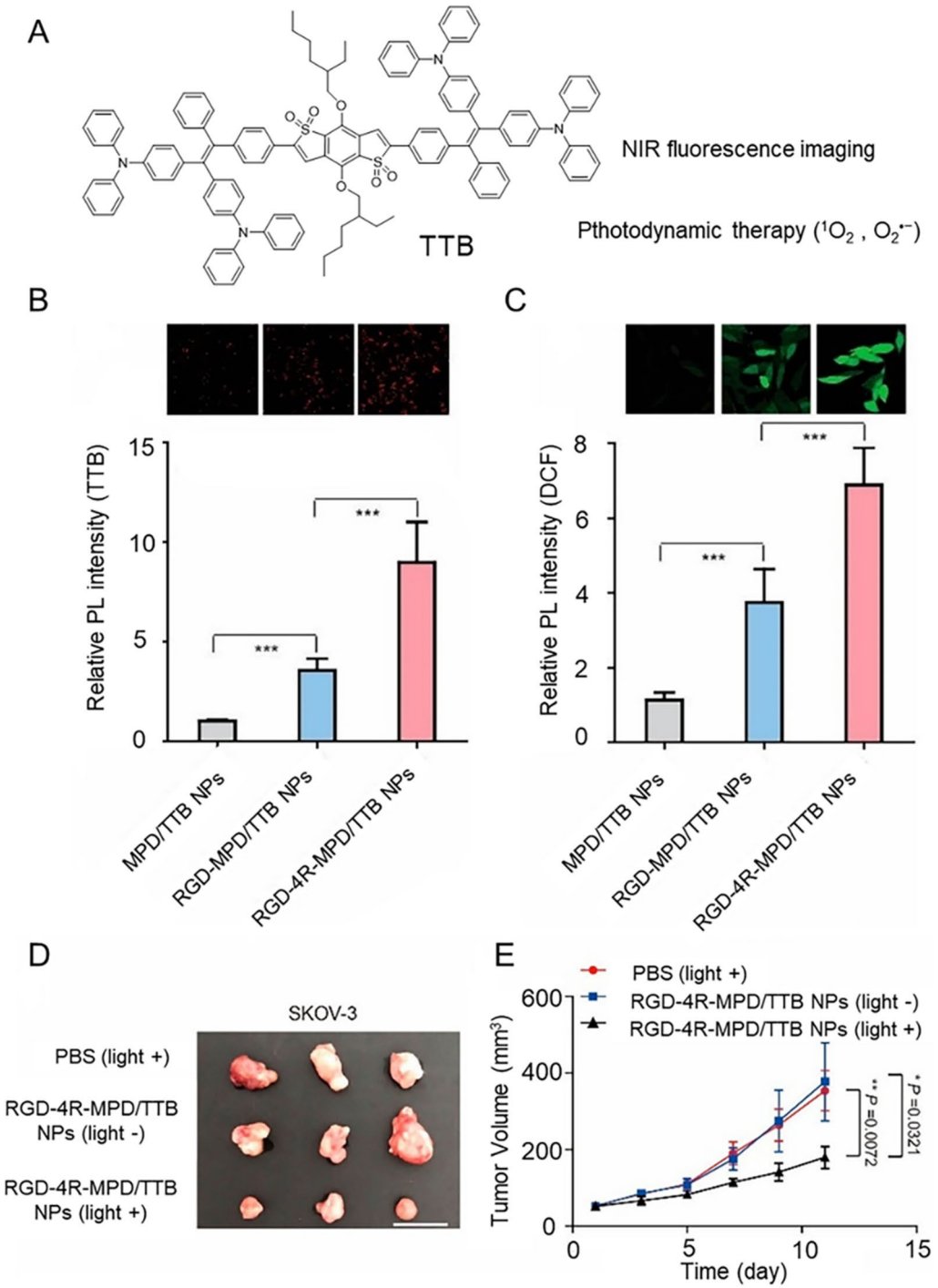

Fig. 6 **A** Structure of TTB. **B** The relative PL intensity of SKOV-3 cells incubated with NPs. **C** Detection of intracellular ROS generation by DCFH-DA in SKOV-3 cells. **D** Tumor images, **E** tumor volume changes of SKOV-3 tumor-bearing mice after photodynamic therapy. Data were reported as mean ± SD and analyzed by two-sided Student's t-test. *P < 0.05, **P < 0.01, ***P < 0.001, *n.s.* = not significant. Reproduced with permission [115]. Copyright 2020, American Chemical Society

Cervical cancer

Cervical cancer is the fourth commonest cancer in the world, which seriously affects women's life and health. Although it can be defended against with the HPV vaccine, persistent high-risk human papillomavirus (hrHPV) infection is the main cause of cervical cancer [119]. At present, the main treatment for cervical cancer includes radiotherapy, laser-based ablation, surgery and cold coagulation etc., but it still has many side effects [120]. PDT is extensively used in the treatment of malignant tumors due to its small trauma. A study on topical MAL-PDT reported that 75% (42/56) of cervical intraepithelial neoplasia (CIN) presented complete responses to MAL-PDT. For patients with CIN 2 and CIN 3, 90% are cured after two to three years of treatment [121]. Another article reported the topical administration of HAL suppositories in 47 patients with CIN 1 [122]. The results revealed that 57% of patients in the HAL-PDT group had resolution of CIN lesions at 6 months after PDT, compared with only 25% in the combined control group.

Several different combination therapies have shown excellent anti-cervical cancer efficacy, among which gene therapy (GT)/PDT is widely used. TTC-L-M-4/DOPE was prepared by Liu and Yang et al., and used to transfer siRNA (p53) with good results, indicating that gene silencing effect was better than Lipo2000 [123]. Meanwhile, TTC-L-M-4 had the ability to effectually produce ROS under light irradiation. Experiments in HeLa cell lines proved that p53 gene therapy combined with PDT greatly improved the efficacy of tumor therapy. Moreover, TTC-L-M-4/DOPE/p53 was injected into HeLa orthotopic tumor-bearing mice subcutaneously, and irradiated for 30 min, 24 h after injection, showing more effective tumor inhibition ability than other groups. Based on the same design principle, Tang et al. proposed a promising strategy for gene delivery in HEK293T cell lines [124]. Finally, combined with PDT therapy to achieve synergistic therapy, the killing effect on cancer cells was significantly enhanced. Tang et al. synthesized the PDT drug TBP-Au to avoid overexpression of the antioxidant system in cervical cancer [125]. Thioredoxin Reductase and its natural substrate, Thioredoxin, were one of the major antioxidant systems in cells, and inhibition of Thioredoxin Reductase will stimulate ROS production and induce apoptosis. The Au complex can effectively inhibit Thioredoxin Reductase, and the AIE-PS (TBP) can achieve imaging guidance and the specific treatment of ROS. The synergistic therapy of Au complex and TBP on Hela tumor-bearing nude mice under light displayed the ability to treat cervical cancer accurately.

Specific targeting of cervical cancer cells brings benefits for improving therapeutic efficiency. By recognizing the FA receptors (overexpressed in HeLa cells), Wen et al. synthesized FFM1 to target HeLa cells specifically, which showed outstanding capacities in target imaging and photodynamic killing of HeLa cells [126]. Targeting subcellular organelles can also effectively promote PDT. For example, Jiang et al. proposed a simple AIEgen, IQ-TPA, with mitochondrial targeting [127]. Preferably, it had bright two-photon fluorescence, enabling image-guided PDT with deeper penetration of tumors. All of this was demonstrated in HeLa cells. We know that the nucleus is identified as an ideal target for anti-tumor treatment because the DNA and some certain enzymes in the nucleus are the major causes of cancer and malignant proliferation. Wang and his collaborators developed MeTPAE, a nuclear targeting material [128]. MeTPAE can not only interact with histone deacetylases (HDACs) to suppress the proliferation of Hela cells, but also accurately destruct telomeres and nucleic acids via PDT, providing a new opportunity for the effective treatment of malignant tumors.

In order to effectively simplify cancer treatment, Zhang et al. developed multifunctional AIE-PSs [129]. As shown in Fig. 7, PS1 NPs were prepared by encapsulating PS1 into polymers, which exhibited bright red-emission, high quantum yield, good biocompatibility and suitable $^1O_2$ generation ability. What's more, PS1 NPs incubated with HeLa cells with only gentle shaking for 5 s at room temperature to strongly illuminate the cytoplasm, showing ultra-fast staining and mild incubation conditions of PS1 NPs. Meanwhile, PS1 NPs could track cells for more than 14 days, demonstrating long-term tracking ability. Although the fluorescence intensity of U14 tumor-bearing mice decreased gradually, it still maintained at 42% of the initial intensity after 14 days. The relative tumor volume in the control group increased 10–13 times after 14 days, suggesting that radiotherapy alone or PS1 NPs had little effect on tumor growth. As expected, the tumor volume was significantly reduced in the PS1 NPs in white light irradiation group. This work resulted in an AIE-PS that combines image-guided PDT, ultra-fast staining, and long-term tracking capabilities, offering huge advantages for the clinical applications.

(See figure on next page.)

Fig. 7 **A** Structural formulas of PS1 and PS2 and schematic illustration of PS1 NPs as PSs for "all-in-one" PDT. **B** Time-dependent fluorescence images of U14 tumor-bearing mice after intratumoral injection with PS1 NPs or with PS1 NPs + white light. **C** Tumors collected from different treatment groups. **D** Tumor volume changes by different treatment methods. (***P < 0.001, PDT *vs*. other groups). Reproduced with permission [129]. Copyright 2020, Royal Society of Chemistry

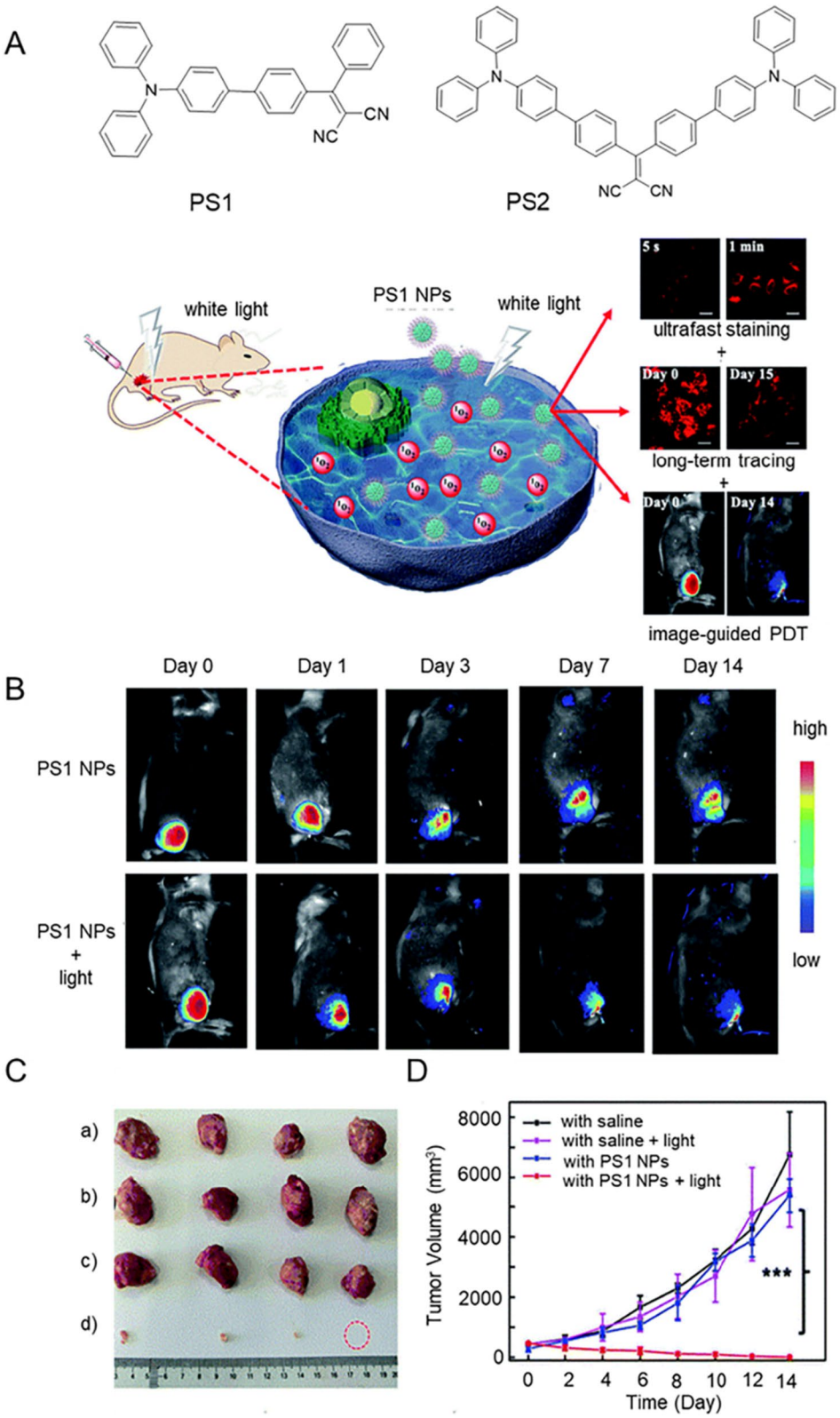

Fig. 7 (See legend on previous page.)

Brain cancer

There are more than 120 types of brain tumors, and approximately 45% of primary brain tumors are gliomas, of which glioblastoma multiform (GBM) is the most common and aggressive tumor [130]. Regrettably, there are few effective treatments for these cancers, and the median survival rate for glioblastoma patients is only 14 months, even after aggressive surgery, chemotherapy and radiotherapy [131]. Chemotherapy is one of the most commonly used treatments for gliomas [132]. Unfortunately, the indiscriminate cytotoxicity of chemotherapy can lead to serious side effects as they fail to distinguish cancer cells from healthy cells, inhibiting fast-growing normal tissues and cells. Tumor cells are resistant to multiple other unexposed antitumor drugs with different structures and targets, which leads to multidrug resistance (MDR) in the treatment process. [133–135]. Such nonspecificity hinders the effect of chemotherapy and impairs the inhibition of tumor growth, metastasis, and recurrence [136–139]. With the innovation of treatment technology, it is possible to reduce the disadvantages of chemotherapy in cancer treatment, so that brain cancer can be better treated.

Appropriate brain imaging methods and corresponding excellent contrast agents are prerequisites for brain tumor treatment, which require good sensitivity and specificity, deep penetration, and high spatial and temporal resolution. Liu's group reported a novel NIR-II fluorescent molecule (TB1) with AIE property for in situ imaging of brain tumors [140]. TB1 was encapsulated in a polymer matrix and further modified with c-RGD to obtain targeted AIE dots, showing selective and specific tumor uptake, with a high signal/background ratio of 4.4 and a resolution up to 38 μm. More importantly, precise tumor-depth detection was achieved through non-invasive PA imaging of orthotopic brain tumors via the intact scalp and skull. To improve the resolution, Gao and Li collaborated to fabricate an albumin-based AIE nanoprobe, which has realized actively targeted NIR-II imaging of brain tumors and cerebrovascular imaging in a high-resolution (~70 μm) mouse model [141]. This provides a prerequisite for fluorescence imaging-guided surgery for cerebral ischemia and brain tumors, improving surgical efficacy and preventing recurrence and side effects.

To circumvent the problems of chemotherapy, new therapies combining PDT and chemotherapy can efficiently eliminate extensive cancer cells and introduce minimal potential into MDR [142–144]. Guo and Wu skillfully combined AIE fluorophore and cisplatin to prepare mitochondria-targeted photosensitizer (TNPT) with AIE properties for collaborative antitumor therapy [145]. The chemotherapeutic efficacy of TNPT is similar to that of cisplatin, but its ability to generate ROS is higher than that of Ce6. In addition, TNPT has better biocompatibility than free cisplatin, significantly reduces cytotoxicity to normal cells, and shows selective uptake from cancerous cells rather than normal cells. Most importantly, TNPT has synergistic photodynamic and chemotherapy effects on C6 glioma cells, and was 2.4 times more effective than cisplatin under 15 J cm^{-2} white light irradiation (Fig. 8).

Another obstacle to glioma therapy is that the drug delivery system must cross different biological barriers during treatment, especially the blood–brain barrier (BBB) and blood-tumor barrier (BTB) [146]. Transferrin receptor (TfR) overexpression has been reported to exist in brain capillary endothelial cells and many malignant tumor cells [147]. In response, the T7 peptide was selected by Hu and Zhou et al. to design a delivery system across the blood–brain barrier because of its similar affinity with transferrin [148, 149]. An amphiphilic polymer (PLA-PEG-T7/TPE) with AIE properties was successfully constructed for drug delivery in tumor therapy. Finally, the drug TMZ was encapsulated into PLA-PEG-T7/TPE to construct nanoparticles (PLA-PEG-T7/TPE/TMZ). The inhibition of cell proliferation suggested that the drug micelles had dose-dependent cytotoxicity to LN229 cells. Meanwhile, the therapeutic effect of PLA-PEG-T7/TPE/TMZ was the best in the in vivo anti-tumor experiments.

Brain-targeting apolipoprotein E peptide (ApoE) is a targeted functional peptide that promotes effective BBB penetration [150]. Brain-targeted near-infrared IIb (NIR-IIb) AIE nanoparticles were developed by Wang et al., and ApoE was then grafted onto these nanoparticles, termed ApoE-Ph NPs [151]. A band-pass filter with a wavelength of 1550 nm could be utilized to monitor the in vivo biological distribution and accumulation of nanoparticles in an in-situ glioma model, overcoming previous limitations in wavelength range and equipment. Under 808 nm laser irradiation, ApoE-Ph NPs exhibited high PTT efficiency and significantly improved the survival rate of in-situ GBM mice. Fortunately, recent clinical studies have shown that immune cells can perform immune surveillance in the central nervous system to cross the blood–brain barrier. Even more impressively, Natural killer (NK) cells represent a variety of proteins for tumor recognition and has been considered for cancer immunotherapy. Deng and his collaborators developed a natural-killer-cell-mimic nanorobots (NK@AIEdots) by covering the AIE-active polymer endoskeleton PBPTV with NK cell membranes [152]. It is noteworthy that NK@AIEdots can pass through the BBB in a self-help manner and specifically accumulate in the complex brain stroma of brain

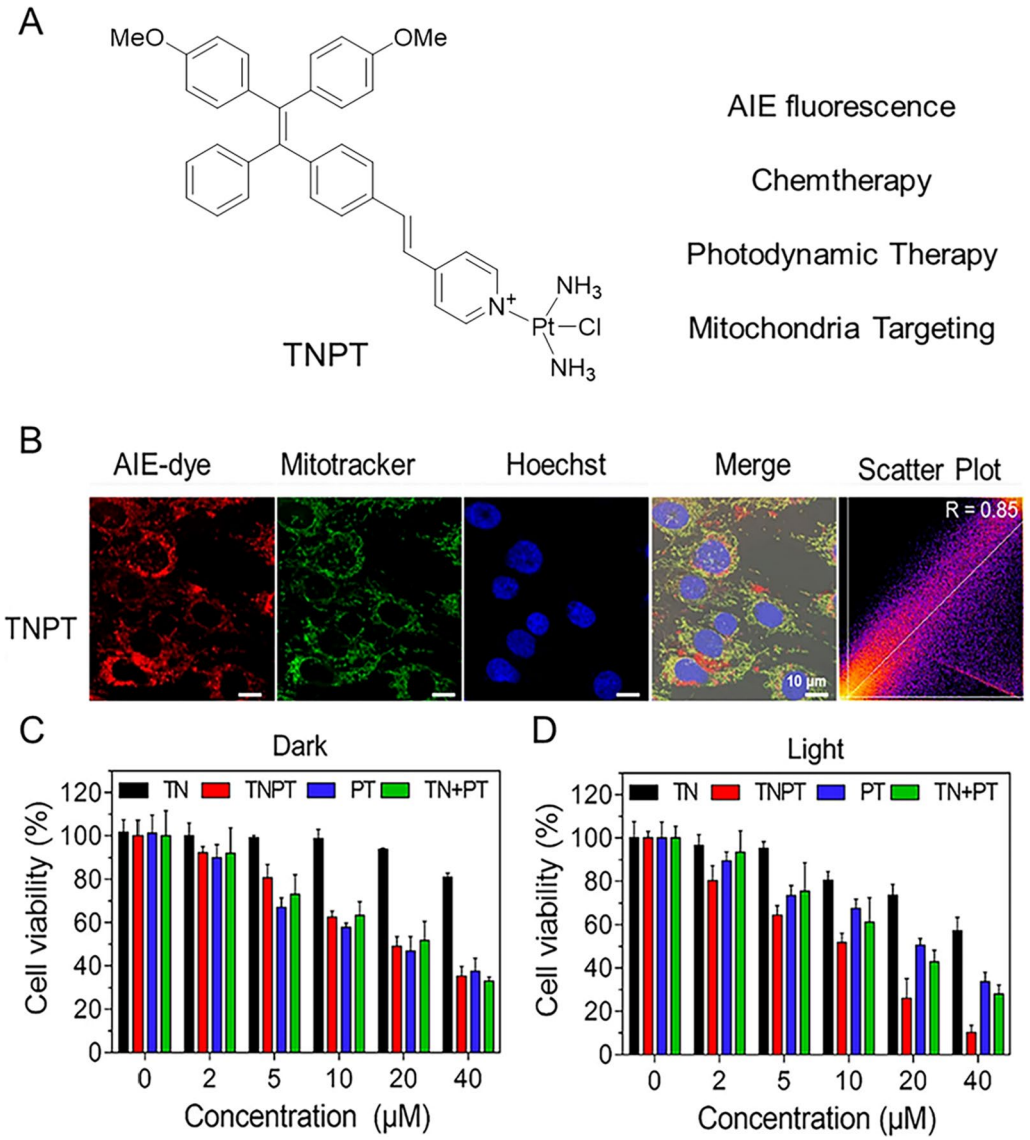

Fig. 8 **A** Structure of TNPT. **B** CLSM images and overlapping coefficients shown in frequency scatterplots of C6 cells incubated with TNPT (5 μM) for 2 h. **C** Inhibitory effects of TN, TNPT, PT, and TN + PT on the C6 cell under dark and **D** light irradiation (15 J cm^{-2}) at 50 mW cm^{-2} for 5 min. Reproduced with permission [145]. Copyright 2020, American Chemical Society

tumors. This greatly improves the efficiency of in situ transcranial-scalp fluorescence imaging and PTT. It turns out that these NK@AIEdots did greatly inhibit tumor growth under NIR light. All of these strategies show great potential in active transmission of BBB, which lays a foundation for the treatment of brain cancer.

Skin cancer

There are two types of skin cancer, including malignant melanoma (MM) and non-melanoma skin cancer (NMSC) [153, 154]. The incidence of both MM and NMSC has increased over the past few decades, and the incidence of all skin cancers is much higher than that of almost any other type of cancer. Cutaneous malignant melanoma (CMM) is the most common, fastest-growing malignancy in Caucasians, and the most aggressive form of all skin cancers diagnosed [155]. Chemotherapy used immediately after the surgery is an essential element and the key treatment modality in the available treatment options for skin cancer. Unfortunately, traditional chemoprevention regimens have major problems with lack of response to treatment and associated side effects [156].

Therefore, much more effective anti-cancer drugs and treatments are needed. Currently, immunotherapy and targeted therapy have been developed, and other treatments are being investigated [157].

MM has a high tendency to metastasize, and once melanoma has spread beyond its original location, surgical treatment becomes extremely difficult, while resistance to conventional chemotherapy and radiation has increased dramatically [158]. Happily, PDT is emerging as an effective way with precise spatiotemporal control for cancer treatment and may be a promising treatment for melanoma. Tang's research group developed an AIE molecule named DCQu, showing extremely high $^1O_2$ generation efficiency and near-infrared two-photon activity [159]. DCQu not only selectively targets cancer cells without using any biomarkers or additional modifications to target ligands, but also specifically stains mitochondria. Under white light irradiation, DCQu showed significant dose-dependent toxicity, with cancer cell viability decreasing to 9% at 10 μM. The survival percentage of mice treated with "Ce6 + light" remained ~ 60% at day 45, while that of "DCQu + light" reached ~ 80%, indicating that the PDT application of DCQu prolonged the survival time of B16 melanoma-bearing mice. In order to more accurately locate melanoma in space, as shown in Fig. 9, Li and Tang jointly proposed that lipid-encapsulated AIE nanoparticles (AIE NPs) could be used as laser imaging agent for spatiotemporal imaging of tumor tissues with penetration depth up to 505 μm in A375 tumor-bearing mice models [160]. Not only that, AIE NPs can simultaneously generate $^1O_2$ and •OH to induce tumor ablation. Finally, AIE NPs could be effectively eliminated from the mice after imaging and treatment.

The incidence of MM is relatively scarce compared to the highest mortality rate of all skin cancers. Among Caucasians, the incidence of NMSC is much higher than that of MM, so the treatment of NMSC also requires further studied [161]. NMSC includes basal cell carcinoma (BCC) and squamous cell carcinoma (SCC), and so on [162]. Wang and Zhu et al. collaborated to develop an AIE-based therapeutic agent (TPA3) that is phototoxic to cancer cells and A431 (human basal cell carcinoma) tumor-bearing nude mouse under irradiation of white light [163]. The photocytotoxicity of TPA3 in cancer cells was detected by MTT assay. Encouragingly, an extremely low concentrations (5 μM) of TPA3 resulted in the death of about 70% of cancer cells after LED irradiation for 10 min, while normal cells were not significantly injured. This fully demonstrated that TPA3 had the advantage of being specifically selective for cancer cells, prompting further exploration in vivo. TPA3 was injected into A431 tumor-bearing nude mouse model 24 h later. By comparing the fluorescence signals of tumor and normal organs, TPA3 was found to mainly concentrate in the tumor site. When the tumor volume reached ~ 50 mm^3, the mice were randomly divided into four groups and given different treatment regimens. TPA3 (100 μL 200 mm^{-3}) was injected into tumor-bearing mice after 30 min of irradiation with LED light (200 mW cm^{-2}, 10 min). Additional illumination was given every 3 days, and the relative tumor volume was measured 14 days later. Compared with other groups (PBS, PBS with light, TPA3), the TPA3 with light group had a significant inhibitory effect on tumors, indicating that TPA3 had a good PDT treatment effect on tumors under LED light. More excitingly, in addition to its effective PDT, TPA3 provides in-situ monitoring of dynamical mitophagy process involving mitochondria, AVs, and lysosomes, which will effectively avoid overtreatment by providing a real-time self-monitoring system for assessing the efficacy of late cell apoptosis.

Lung cancer

Lung cancer is a major cause of cancer-related morbidity and mortality and has been increasing over the past decades, becoming a great challenge for health management department and mankind [164]. Of concern was that lung cancer accounts for about 20% of all cancer diagnoses. Until now, treatment has generally been determined according to the stage of lung cancer. There is little dispute, for example, that surgery is the preferred treatment for stage I to II lung cancer for eligible patients [165]. Radiotherapy is mainly used for early and intermediate non-small cell lung cancer (NSCLC) [166]. Systemic therapy, including chemotherapy, targeted therapy, and immunotherapy, is the dominant treatment strategy for patients diagnosed with advanced/metastatic lung cancer [167]. In line with changes in medical practice related to cancer screening and/or treatment, advances in the treatment of lung cancer has intensified, however, more approaches to treatment must be needed.

The specific recognition of overexpressed antigens on the surface of lung cancer cells provides a great opportunity for accurate diagnosis and treatment of lung cancer. Cetuximab (C225) has been proved to be an effective therapeutic agent by specifically targeting EGFR factors overexpressed in lung cancer [168]. Based on the high

(See figure on next page.)

Fig. 9 **A** Structure of TPE-PTB and AIE NPs for TPFI guided PDT application. **B** Two-photon 3D reconstructed images of the tumor tissue. **C** Photograph of the resected tumors in different treatment groups. **D** Tumor growth curve during the treatments. The data show significant statistical difference between the laser irradiation group after AIE NPs-treatment and the laser irradiation group after PBS treatment. (*P < 0.05). Reproduced with permission [160]. Copyright 2020, American Chemical Society

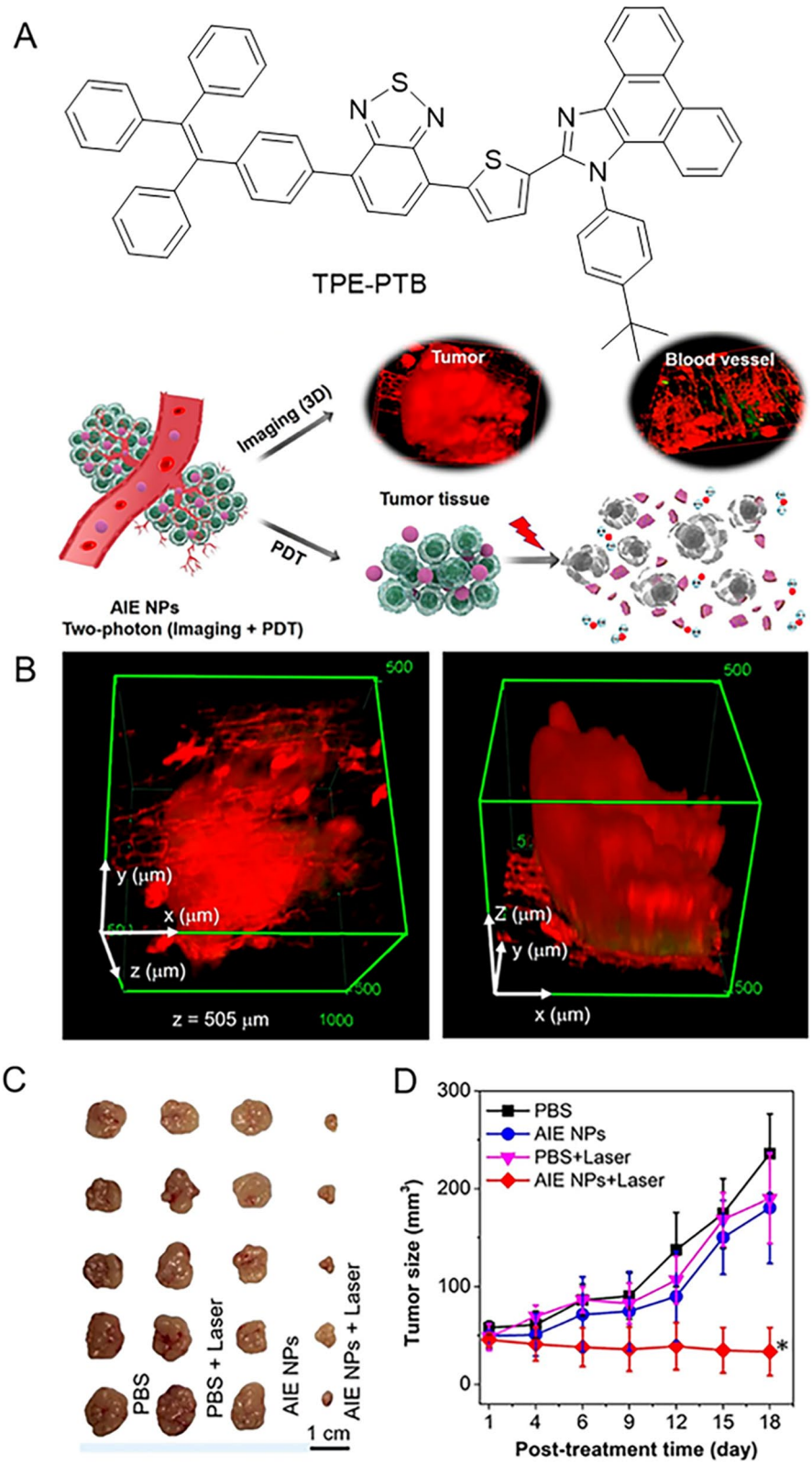

Fig. 9 (See legend on previous page.)

specificity and affinity of C225, *t*-BuPITBT-TPE-C225 NPs were obtained by modifying *t*-BuPITBT-TPE encapsulated in biocompatible DSPE-PEG with C225 [169]. *t*-BuPITBT-TPE-C225 NPs can be used to target non-small cell lung cancer cells, which has been validated by confocal microscopy and flow cytometry experiments. Su et al. also utilized C225 coupled with TPENI NPs to achieve specific fluorescence imaging and detection of non-small lung cancer cells [170]. Low-density lipoprotein receptor (LDLR) that was typically upregulated in A549 cells (Human non-small cell lung cancer cells), was also a target for cancer cells. Based on this, Wang et al. designed and synthesized a novel AIE-PS (TPA-DPPY) that generates ROS under white light irradiation and specifically encapsulated it into low-density lipoprotein (LDL) particles as a PS for photodynamic killing of A549 cells [171]. According to quantitative analysis of cell viability data, TPA-DPPY exhibited obvious phototoxicity to A549 cancer cells, with killing efficiency up to about 88%. Interestingly, the ROS generation process is accompanied by significant changes in TPA-DPPY luminescence, such as enhanced luminescence and blue shift emission, allowing real-time fluorescence monitoring of the PDT process. This capability is extremely important because it provides immediate feedback on treatment outcomes and has great potential in a multifunctional PDT.

Metallic drugs have been used to treat cancer for more than 50 years, since the advent of cisplatin [172]. However, cancer cells can develop metal drug resistance after multiple rounds of treatment, greatly limiting the efficacy of treatment, which is no exception for lung cancer treatment [173]. To overcome cisplatin resistance, Su et al. proposed a new strategy to solve the problem through mitochondrial dysfunction according to the anticancer mechanism of cisplatin (cis-Pt) [174]. Two mitochondria-targeted AIE molecules, DP-PPh_3 and TPE-PPh_3, demonstrated superior ability to overcome cisplatin resistance in lung cancer cells (A549R) by altering drug metabolism (up-regulation of influx CTR1 and down-regulation of efflux MRP2) and blocking autophagy flux (failure of the degradation of autophagosomes). Meanwhile, DP-PPh_3 and TPE-PPh_3, acting as PSs, could induce ROS production, resulting in the destruction of mitochondrial structure and impaired glycolytic metabolism. In addition, the anticancer effects of these two molecules were verified in 3D multicellular tumor spheroids (MCTSs) of A549R cells and tumor-bearing nude mice. This strategy not only promotes the PDT effect on cancer cells, but also provides a new pathway to drug resistance for metal drug therapy.

More photosensitizers are being developed to treat lung cancer, Deng et al. developed an AIE-PS BODIPY-TPA, which could be transformed into relevant nanoparticles (BODIPY-TPA NPs) through self-assembly process, and further studied the photodynamic toxicity of the particles to A549 cells [175]. It was confirmed that the IC50 of BODIPY-TPA NPs was 28.45 μg mL^{-1} under a single laser irradiation of 635 nm. Zheng and collaborators prepared an NPs-targeting mitochondria using a novel AIE cross-linked copolymer (PAIE-TPP), which was highly cytotoxic to A549 cancer cells with a survival rate of only 4% under an ultralow white light power intensity of 10 mW cm^{-2} [176]. These results indicate that particles coated with AIE-PSs can be used as a class of safe and multifunctional nano phototherapy drugs in the field of

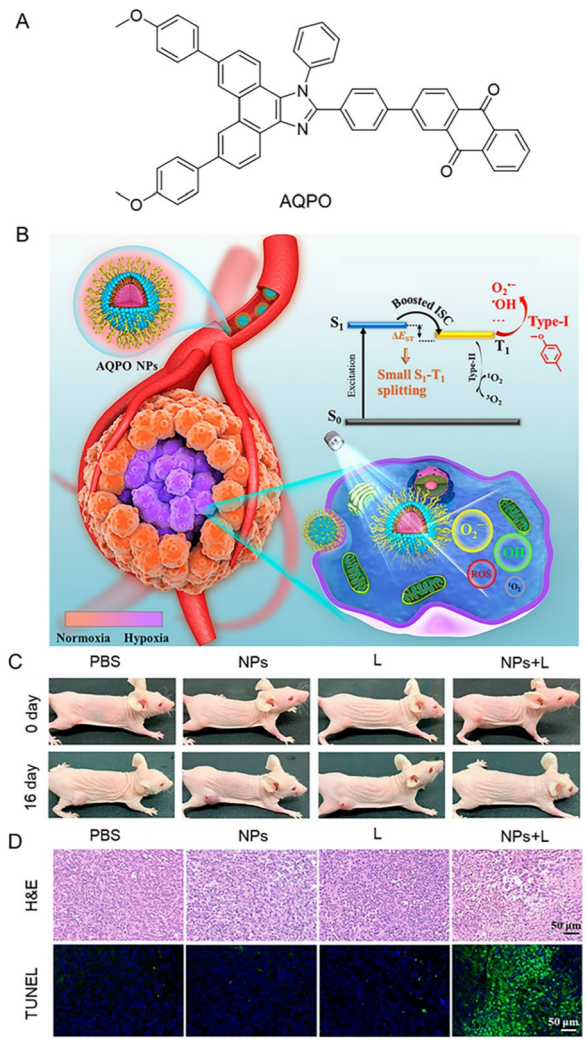

Fig. 10 **A** Structure of AQPO. **B** Schematic diagram illustration of AQPO NPs for cancer treatment. **C** Pictures of A549 tumor-bearing mice in different treatment groups on the 0 day and 16th day, respectively. **D** H&E and TUNEL staining of tumor sections of mice in different treatment groups. Reproduced with permission [177]. Copyright 2022, American Chemical Society

PDT for lung cancer cells, which has become the basis for further exploration in clinical experiments.

Based on the great advances in AIE-PSs at the cellular level, the researchers continue to study its effects in A549 tumor-bearing mice. As shown in Fig. 10, Xiao et al. demonstrated the synthesis of a novel AIE (AQPO) and its assembly of nanoparticles (NPs) to promote the increase of O^{2-} and •OH generation efficiencies [177]. Using A549 tumor-bearing mice as models, they investigated the PDT effect of AQPO NPs in vivo. Mice were randomly divided into 4 groups: PBS, PBS + light (L), AQPO NPs (NPs) and AQPO NPs + light (NPs + L). After 16 days of different treatments, significant suppression of tumor growth was observed in the group of NPs + L, compared with PBS, L and NPs groups, which was mainly due to its superior PDT and hypoxia-overcoming effect of AQPO NPs. Meanwhile, H&E staining showed that the NPs + L group exhibited more apoptotic and necrotic cells compared with the other three groups. These results further indicated that AQPO NPs could effectively eliminate tumor cells under white light irradiation and had the excellent anti-hypoxia PDT effect. In addition, Cao et al. constructed a biodegradable polymer with AIE characteristics, which had mitochondrial targeting ability [178]. This polymer improved the efficiency of co-encapsulated photosensitizers and the therapeutic index of cancer cells in vitro and in vivo, contributing to the photodynamic therapy of lung cancer.

Breast cancer

According to the latest data from the American Cancer Society, which estimated the numbers of cancer cases and deaths in the United States, the incidence of breast cancer in women continued to rise slowly (0.5% per year) between 2014 and 2018 [179]. Despite encouraging advances in breast cancer treatment and related 5-year survival outcomes, the treatment of metastatic breast cancer remains a major challenge [180]. For breast cancer diagnosed locally, which accounts for approximately 90% of all cases, the main treatment is surgery to achieve complete resection of the primary tumor [181]. However, even the most advanced surgeries and treatments can not prevent breast cancer recurrence and metastasis. Therefore, the first step in local treatment of cancer cells is surgical resection, usually followed by radiation therapy of the tumor bed [182]. Finally, Systemic drug therapy is administered with the aim of eliminating any residual cells to prevent metastatic recurrence. Although the current standard of treatment includes a combination of surgery, radiation and drugs, other treatments need to be introduced to treat breast cancer completely [183–185]. The excellent performance of PDT in clinical practice has undoubtedly become an interesting new research approach.

Currently, surgical resection is the most direct way to treat solid tumors, but small lesions remain after treatment. Therefore, combined with PDT after resection is a favorable choice to cure the disease. In collaboration with Dai et al., Jiang developed a single AIE molecule to achieve NIR fluorescence surgical navigation in breast cancer mice, and some microscopic residual tumors are further completely ablated by PDT and PTT to maximize the death of tumor cells and tissues. With this combination of image-guided surgery, PDT and PTT, survival rates of up to 90% can be achieved [186]. Besides, there is a great demand for therapeutic anticancer drugs with multiple therapeutic functions for breast cancer. Platinum (Pt)-based anticancer drugs are still commonly used chemotherapy drugs in the treatment of breast cancer. Non-toxic Pt(IV) prodrugs have been subsequently developed, and are widely used due to their reduced side effects. Su and collaborators developed a triphenyl phosphorus (TPP) modified AIE-based Pt(IV) prodrug ACPt, which was for the image-guided chemotherapy [187]. ACPt has high cytotoxicity to human breast cancer cells and can induce the increase of ROS. Specifically, the toxicity of ACPt to MCF-7 cells was about 2.5 times that of free AC ligand, and around 5.5 times to the CDDP, suggested that ACPt has a strong synergistic effect on MCF-7 cells. Furthermore, the combination of PDT and PTT showed promising advantages in the treatment of breast cancer. Two novel AIE-active fluorinated compounds, DPMD and TPMD, had been designed by Liu et al. [188]. Taking TPMD as an example, nanoparticles were constructed by encapsulating it into amphiphilic polymer F12, named as TPMD NPs. It is noteworthy that TPMD NPs had a great advantage in PDT due to their efficient production of ROS, while their excellent photothermal effects could be used for photothermal imaging, photoacoustic imaging, and PTT. The cooperation of PDT and PTT is considered as successful system in synergistic cancer therapy to achieve synergistic effects with boosted therapeutic outcomes [189, 190]. The main reason is that the PDT efficacy can be photothermally enhanced, wherein the PTT could improve the oxygen supply in the tumor tissue through raising the blood flow rate, which conversely further eliminates the heat-resistant tumor cells in PTT [191]. It was found that combining TPMD NPs injection with laser irradiation (650 nm NIR laser, 600 mW cm^{-2}) at 24 h postinjection, the tumors of 4T1 tumor-bearing mice were completely eliminated at day 2 after treatment, without recurrence or regeneration. This fully indicated that AIE had high efficiency in the treatment of PDT and PTT combination therapy, and sufficient clinical application potential. Aiming at multifunctional therapy that achieves the comprehensive function of multi-diagnostic imaging and synergistic therapy,

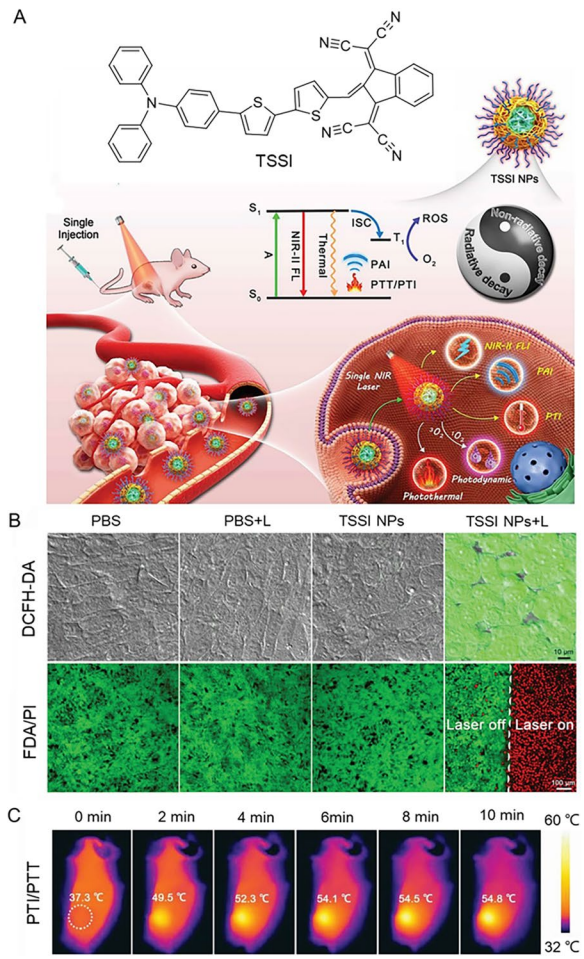

Fig. 11 **A** The structure of TSSI and the process of TSSI NPs in the treatment of tumor with PDT-PTT synergistic therapy under the guidance of NIR-II FLI-PAI-PTI trimodal imaging. **B** Intracellular ROS level and live/dead cell staining of 4T1 cells after treatment under different conditions. **C** Thermal images, heating temperatures (at tumor sites) of 4T1-tumor-bearing BALB/c nude mice during continuous NIR irradiation at 12 h postinjection of TSSI NPs. Reproduced with permission [192]. Copyright 2020, Wiley–VCH

Zhang et al. ingeniously designed and constructed a simple and mighty "one-click" therapy based on an AIE-active PS (TSSI) [192]. It exhibited bright NIR-II fluorescence emission, high photothermal conversion efficiency and highly efficient ROS generation (Fig. 11). The unprecedented performance of PDT-PTT co-therapy guided by NIR-II fluorescence imaging (FLI)-photoacoustic imaging (PAI)-photothermal imaging (PTI) trimodal-imaging was confirmed by the diagnosis of 4T1 tumor and the outcomes of complete tumor elimination.

Human epidermal growth factor receptor 2 (HER2) is over-expressed in more than 20% of breast cancer cases. Therapies targeting HER2 have yielded unparalleled clinical benefits for a subset of breast cancer patients. Zhang et al. successfully applied supramolecular materials and transformable peptides to control HER2 signaling in breast cancer cells [193]. In vivo study of MCF-7/C6 and BT474 xenograft models in mice had shown that this therapy is effective in treating HER2 + breast cancer xenografts. In addition, nanoparticles formed by AIE-PSs contribute to PDT for breast cancer. Liu et al. encapsulated a single AIE-PS into F-127 to form nanoparticles (TBTDC NPs), which exhibited good biocompatibility, highly specific targeting of lysosomes, and impressive tissue penetration (up to 300 μm) [194]. Cell viability of MCF-7 cells incubated with TBTDC NPs was detected via CCK-8 assay. The results indicated that the cell survival rate of TBTDC NPs was about 11% after 10 min of white light irradiation (50 mW cm^{-2}) at a relatively low concentration (12.5 μg mL^{-1}), confirming the excellent potential of TBTDC NPs in PDT for cancer cell ablation. The PDT effect of TBTDC NPs was further investigated in MCF-7 tumor-bearing nude mice. According to the experimental results, the tumor growth of TBTDC NPs with irradiation group was significantly inhibited compared with other control groups after 14 days of treatment. Huang et al. also prepared single AIEgen nanoparticles (BTZPP-NPs) with high-efficiency PDT, which could selectively target lysosomes in living cells with high contrast and up to 14 days of tracking ability [195]. In addition, 63% anti-tumor inhibition rate was obtained in the 4 T1 tumor-xenograft model experiments.

Colorectal cancer

Colorectal cancer (CRC) is the third leading cause of cancer death in both men and women, with an estimated 52,980 deaths in the United States in 2021 [196]. According to estimates, 10.5% of new colorectal cancer cases occur in people under the age of 50, which is increasingly younger [197]. Specifically, from 2000–2002 to 2014–2016, the incidence of colorectal cancer (specifically adenocarcinoma) in adults aged 40–49 has increased by nearly 15% [198]. Currently, there are many types of screening diagnostic methods for CRC, including guaiac fecal occult blood test (gFOBT), fecal immunochemical test (FIT) for hemoglobin, optical colonoscopy (OC) and flexible sigmoidoscopy (FS), etc. [199]. Surgery is the main treatment for localized disease, and combined with postoperative chemotherapy can reduce disease recurrence, especially if the disease has spread to the lymph nodes [200]. Radiation therapy, usually used in combination with chemotherapy before surgery, is one of the main treatments for CRC [201].

CRC fails to be diagnosed and treated early mainly because of the lack of specific/sensitive biomarkers

for early detection. Shen and Tao et al. collaborated to report a mitochondrion-targeted TPE-IQ-2O with AIE property based the differential diagnosis of tumor and non-tumor cells in colorectal tissue, which lay the foundation for treatment of CRC [202]. Furthermore, due to the limited efficacy of conventional treatment, advanced CRC has poor prognosis with high risks of metastasis and recurrence. For the past few years, prominent progress has been made in the development of new treatments for diseases, among which PDT is a promising radical treatment for CRC [203]. Yang et al. reported that cationic luminescent progenitor TPE-DQN, with AIE properties, specifically stained mitochondria within cancer cells, helping them to differentiate cancer cells from normal cells [204]. Under white light irradiation, TPE-DQN could effectively $^1O_2$ and the efficiency is up to 0.83. The advantages of PE-DQN lay the foundation for image-guided PDT to treat cancer cells and inhibit tumors. The observation in CT26-colon tumor-bearing mice further confirmed the therapeutic efficacy of TPE-DQN in vivo. For example, intratumoral injection of TPE-DQN followed by white light irradiation could entirely suppress tumor growth in mice after 10 days of treatments, while intratumoral injection of normal saline had no effect on tumor inhibition regardless of white light irradiation or under dark. TPE-DQN without light irradiation also showed no inhibition of tumor growth. Meanwhile, the body weight loss of each group was negligible during PDT. These phenomena were sufficient to indicate that TPE-DQN could be used as a highly biocompatible PS to inhibit tumor growth through PDT effect.

Activated by long wave light, PSs can minimize tissue decay and kill cancer cells without causing irreversible damage to normal cells. Therefore, the excitation wavelength of PSs for CRC treatment is mainly concentrated in the NIR, even reaches the NIR II. Gao et al. designed a series of PSs by adjusting the steric hindrance of molecules [205]. Among them, NIR-II PS nanoparticles prepared by BNET and albumin exhibited high-efficiency $^1O_2$ generation, good photostability, as well as negligible dark toxicity. As shown in Fig. 12, The nanoparticles demonstrated highly specific NIR-II fluorescence imaging as well as efficient image-guided PDT in mice with in situ colon cancer or pancreatic cancer. The engineered nanoparticles revealed great potential in biomedical applications. In addition, the specific microenvironment of the tumor region becomes the trigger condition that can activate the PSs for CRC. For example, Min et al. reported a water-soluble AIE-PS with high targeting ability based on the acidic microenvironment of tumors [206]. Notably, the reversible control of $_1O^2$ production and photodynamic targeting of cancer cells in cultured and tumor-bearing mice in an acidic environment (pH 5.2) were permitted. Furthermore, the concentration of glutathione (GSH) in tumors is much higher than in normal tissues, which is considered to be a prerequisite for PS activation. Zhang et al. designed a novel ferrocene-modified vinyl pyridinium-substituted tetraphenyl ethylene (TPEPY-S-Fc) with disulfide bonds as an activated PS for GSH [207]. The fluorescence and $_1O^2$ generation of TPEPY-S-Fc were blocked in the presence of ferrocene. When GSH is encountered, the S–S bond breaks and the PDT-active Tpepy-SH species is released. Finally, TPEPY-SH can induce CT-26 cells apoptosis by generating $_1O^2$ under light irradiation.

Prostate cancer

Prostate cancer is reported to be one of the main causes of death in men in the United States and the second most common type of cancer diagnosed in men worldwide [179, 208, 209]. Notably, the 5-year survival rates for patients with prostate cancer are variable and depend on clinical stage. According to the American Cancer Society (cancer.org), men with localized or regional prostate cancer had a 5-year survival rate of nearly 100%. However, for men diagnosed with distal metastasis, the survival rate is only 30%. Currently, localized prostate cancer is treated mainly with surgical removal of the gland or radiation therapy, which has been shown to be feasible [210]. However, for patients at high risk of distal metastasis, hormonal deprivation caused by surgical removal of the gland which leads to castration of resistant prostate cancer (CRPC) is a major clinical challenge [211]. Therefore, the development of medical tools and new treatment methods is of great significance for the timely diagnosis of the diseases.

Local and metastatic recurrence of prostate cancer usually occurs after radical excision of the primary tumor is attempted. Therefore, during surgical excision of prostate cancer, technologies that can improve the visualization of tumor margins and adjunctive therapies to ablate remaining tumor tissue are needed. AIE-PSs possess the potential to combine fluorescence image-guided surgery with PDT to resect and ablate cancer cells [212]. Jayaram synthesized novel TPE conjugated compounds that underwent unique self-assembly to form spherical nanoparticles (TPE-NPs) with a size of 10 ± 5 nm, which displayed AIE emission in the near-infrared region [213]. As shown in Fig. 13, the potential use of TPE conjugated 4 as near-infrared fluorescent probes and PDT agents was investigated. Compared with normal cells, TPE-NPs showed an unusual preference for tumor cells and were localized in the cytoplasm. ROS produced by TPE conjugated 4 in PC3 cells under light irradiation were analyzed as one of the reasons for photoinduced cytotoxicity.

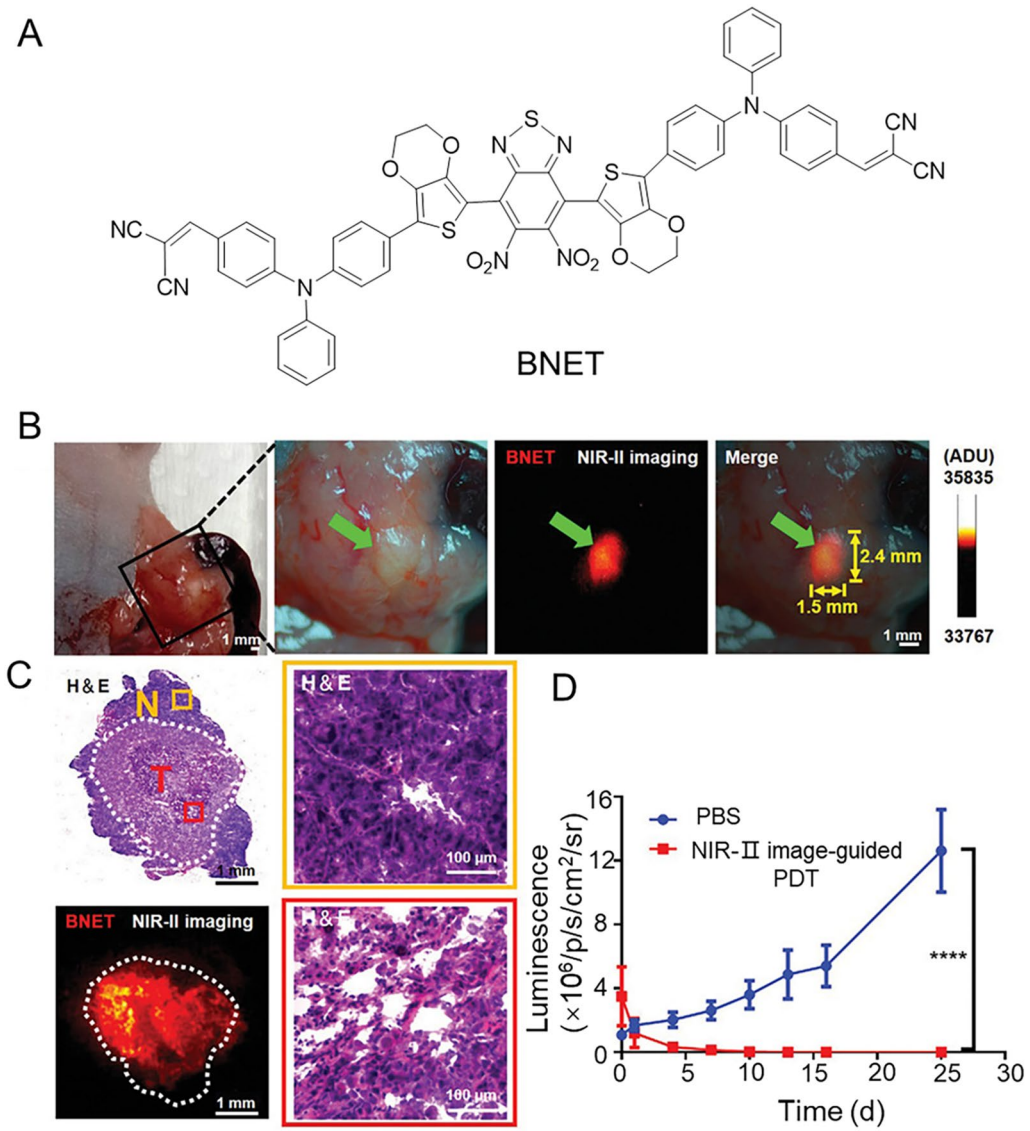

Fig. 12 **A** The structure of BNET. **B** Intraoperative NIR-II imaging of nude mice bearing orthotopic Panc-1-luc pancreatic tumor by BNET NPs. **C** H&E staining and NIR-II real-time imaging of tumor sections. Dotted circles, areas of tumor. T, tumor; N, normal pancreatic tissue. **D** Tumor growth curves after different treatments were measured by the bioluminescence. Data are mean ± SD (n = 5). Significant statistical difference between the NIR-II image-guided PDT group and the PBS group (****p < 0.0001). Reproduced with permission [205]. Copyright 2021, Wiley–VCH

Further evidence of the potential of PDT was obtained using immunodeficient SCID mice implanted subcutaneously with luciferase expressed human prostate tumor cells (PC3) on their backs. In short, the treatment regimen starts after 14 days of tumor cell growth. The mice were divided into 3 groups, in which the experimental group was given TPE conjugated 4 (50 μL, 10 μM) and blue (450 nm) LED lamp irradiation (20 W, 5 min) at the distance of 5 cm. In the other two groups, one group was irradiated at 450 nm for 5 min, while the other was untreated. PLuc activity of the PC3 tumors was monitored weekly by bioluminescence imaging (BLI) and the tumor sizes were measured, followed by continued treatment. The results showed that the tumor volume of the experimental group was observably smaller than that of the other two groups, and the bioluminescence intensity was reduced, indicating that PDT significantly reduced the tumor growth.

Although studies on the use of AIE photosensitizer in the treatment of prostate cancer are currently scarce, PDT therapy has shown promise in the treatment of primary and local prostate cancer after

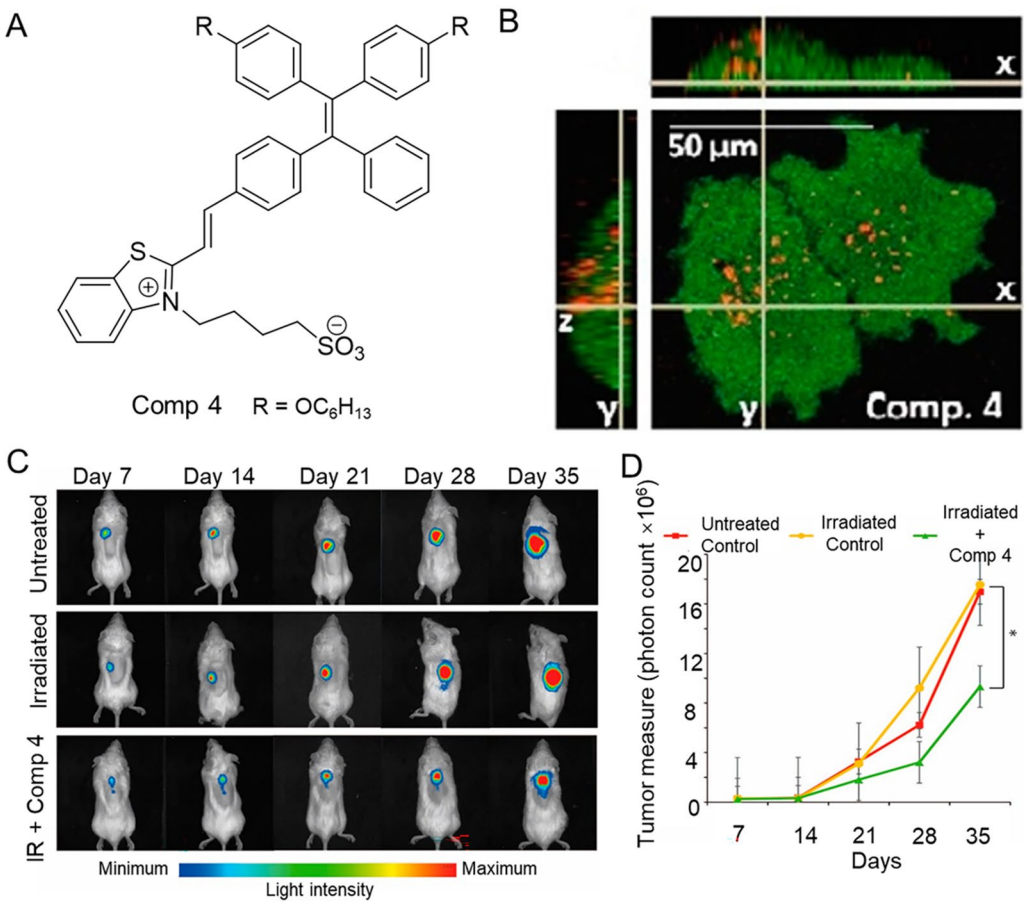

Fig. 13 **A** The structure of conjugate 4. **B** Confocal laser scanning microscopy (CLSM) images of PC3 cell after an overnight incubation with TPE-NPs of conjugate 4, including orthogonal views, left and top rectangular panels. **C** Representative noninvasive bioluminescence images of different treatment groups implanted with PLuc-expressing PC-3 tumors s.c. in SCID mice. **D** Growth response of human PC-3 tumors to different treatment regimens. Reproduced with permission [213]. Copyright 2016, American Chemical Society

radiotherapy. Moreover, the characteristics of prostate cancer can also be used as a reference factor for the design of functional AIE-PSs, in which specific ligand is a very important part, such as FA [214], CD133 antibody [215], cation-independent mannose 6-phosphate receptor [216], prostate-specific membrane antigen (PSMA) [217]. We hope PDT can give full play to its own advantages and provide successful treatment in combination with the characteristics of prostate.

Liver cancer

The liver is the body's largest and most important metabolic organ, which undertakes most of the body's toxin discharge. There are many possible causes of liver cancer, such as obesity, diabetes, fatty liver and so on [218]. Liver cancer is a very serious public health problem with an increasing incidence every year, with 841,000 incident cases and 782,000 mortalities worldwide in 2018 alone [219]. Hepatocellular carcinoma (HCC) accounts for nearly 90% of the primary liver cancer and is the most common type of liver cancer [220]. Currently, the treatment of HCC mainly depends on the diagnosis stage of patients, among which only surgical resection or liver transplantation is performed for patients with Barcelona Clinic Liver Cancer (BCLC) stage 0 or A [221]. In contrast, transarterial chemoembolization (TACE) or transarterial radioembolization (TARE) is recommended for patients with BCLC stage B and C [222]. BCLC stage D is referred to as terminal stage, and the current best treatment is symptomatic treatment with supportive care. With the development of technology, local thermal ablative methods, including microwave ablations and radiofrequency, have been regarded as alternative strategies for HCC treatment in an increasing number of cases [223–225]. However, these existing methods may lead to some adverse complications, such as liver decompensation, bile duct damage, extrahepatic organ injury, etc. [226].

Advanced liver cancer is almost incurable and causes a large number of deaths each year. Therefore, non-invasive long-term cancer cell tracing is an effective and important tool to understand the genesis, development, and evolution of cancer cells. Teng and Chen collaborated to develop the NIR AIE-active polymeric dots (TNZ2tPPI-Tat NPs), which showed ultra-long fluorescence biometric imaging (7 days) in MHCC97-H cells and maintained clear fluorescence signal after 5 generations in three hepatocytes (Lo2, MHCC97-H, Hep 3B) [227]. More importantly, according to in vivo fluorescence imaging, TNZ2tPPI-Tat NPs remained strong brightness within 26 days, which was superior to commercial fluorescent probes Cy5 and AF647, etc. AIE quantum dots not only have excellent performance in liver cancer cell tracking, but also provide potential for the cure of HCC with their effective PDT. TPVRT dots developed by Zhang and his collaborators not only showed excellent ROS production in vitro, but also demonstrated excellent performance of long-term tumor tracking and photodynamic ablation in vivo [228]. HepG2 tumor-bearing mice were randomly divided into four groups, including injection of saline, light irradiation, intratumoral injection of TPVTR dots and light irradiation after intratumoral injection of TPVTR dots. Different treatment regimens are initiated when the tumor volume reaches about 100 to 200 mm^3. The efficacy of PDT up to 22 days in vivo was evaluated based on body weight and tumor size recorded every 2 days of nude mice. The normal saline group grew rapidly, and had no significant difference with other control groups. On the contrary, tumor growth in the light irradiation after injection of TPVTR dots group disappeared significantly after 21 days, confirming the effective PDT efficiency of TPVTR dots in vivo.

Epithelial cell adhesion molecule (EpCAM) is overexpressed in HCC, so anti-EPCAM aptamer is used to functionalize nanoscale surfaces to specifically target liver cancer cells. Dineshkumar et al. fabricated mesoporous silica hollow nanospheres (MSHN) encapsulated by AIE-active polymer (PTPA), which were surface modified with anti-EPCAM aptamers to specifically target Huh-7 cells and were effectively internalized [229]. In addition, integrin $\alpha_v\beta_3$ overexpressed in HCC cells is one of the targets. As shown in Fig. 14, Gao et al. designed and synthesized AIE organic nanodots (T-TPETS) targeting integrin $\alpha_v\beta_3$ for image-guided PDT [230]. We know that sub-organelles targeting HCC cells can also promote PDT therapy. Therefore, Zhao et al. developed two long-wavelength therapeutic probes (DCMT and DCMC) with AIE properties, which are modified with triphenyl-phosphonium cation to actively target the mitochondria of hepatoma cells [231]. HepG2 cells were taken as an example to evaluate the PDT efficiency of DCMT and DCMC. First, the cytotoxicity of probes for cells was assessed after incubation with the compound (0 to 40 μM) in the absence of light for 24 h, showing that the cells were viable. Of concern was that concentration-dependent cell death was observed when cells were irradiated with broadband light (22.7 mW cm^{-2}, 100 min). After treatment with 40 μM DCMT and DCMC, cell viability was decreased by 74% and 61%, respectively. When compared with RB, the PDT effect of the probe was superior to that of RB, indicating that the synthetic probe was more prominent than that of the commercial reagent at relatively low concentrations and was capable to kill more HepG2 cells.

Bladder cancer

Bladder cancer is the second most common genitourinary malignancy that originates in bladder cells. Most bladder cancers are diagnosed at an early stage, when they are highly treatable. From 2011 to 2017, the 5-year survival rate for carcinoma in situ of the bladder (by race and stage at diagnosis) was 96% for all ethnic groups in the United States [179]. But even early-stage bladder cancer can recur after successful treatment. For this reason, bladder cancer patients often require follow-up tests several years after treatment to detect a recurrence. As a result, bladder cancer has the highest cost from diagnosis to treatment.

Currently, cisplatinum-based neoadjuvant chemotherapy (NAC) combined with surgical resection plays a key role in the treatment of bladder cancer, but its toxic and side effects severely limit its applications. Therefore, there is an urgent need to combine different treatment modalities with reduced drug dosages to defeat cancer. To solve this problem, Ding and Wang et al. developed a light-enhanced cancer chemotherapy (PECC) strategy based on multifunctional BITT@BSA-DSP NPs, which had excellent PDT and PTT [232]. At the same time, BITT@BSA-DSP NPs could be effectively taken up by bladder cancer cells and then release Pt (II) under the action of reductase, ensuring the efficacy of chemotherapy (Fig. 15). Most importantly, the study of PECC in vivo in MB49 tumor-bearing mice showed that the BITT@BSA-DSP + laser group had a significant tumor suppressive effect compared with other groups, indicating that PECC has an obvious tumor inhibitory of treatment. In addition, there was no significant difference in body weight growth curve among all groups during treatment. These results confirmed that PECC integrated with NIR FL-guided imaging effectively promoted sensitivity of bladder cancer to cisplatin chemotherapy with minimal side effects. This work provides a promising strategy for improving the sensitivity of multiple of cancer

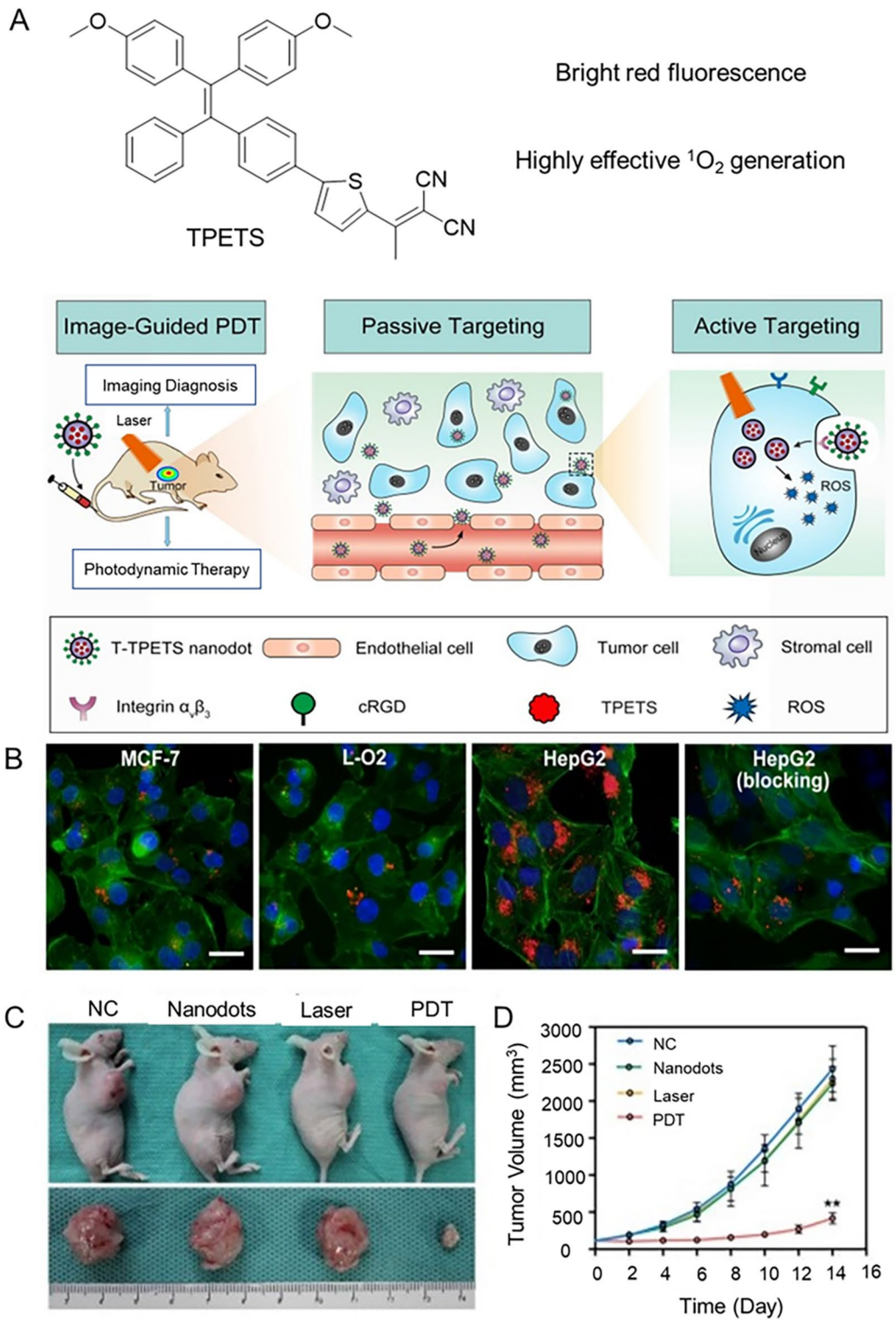

Fig. 14 **A** The structure of TPETS and schematic illustration image-guided PDT mediated by T-TPETS nanodots in xenograft tumor model. **B** Confocal images of MCF-7, L-O2, and HepG2 cells after incubated with the T-TPETS nanodots. Red fluorescence: T-TPETS nanodots. Blue fluorescence: nuclei, green fluorescence: cytoskeleton. Scale bar: 20 μm. **C** Photographs of xenografts and tumors after different treatments. **D** Changes in tumor volume at different time points after treatment in the 4 groups (n = 3 per group). Data represent mean ± SD. Reproduced with permission [230]. Copyright 2019, Ivyspring International

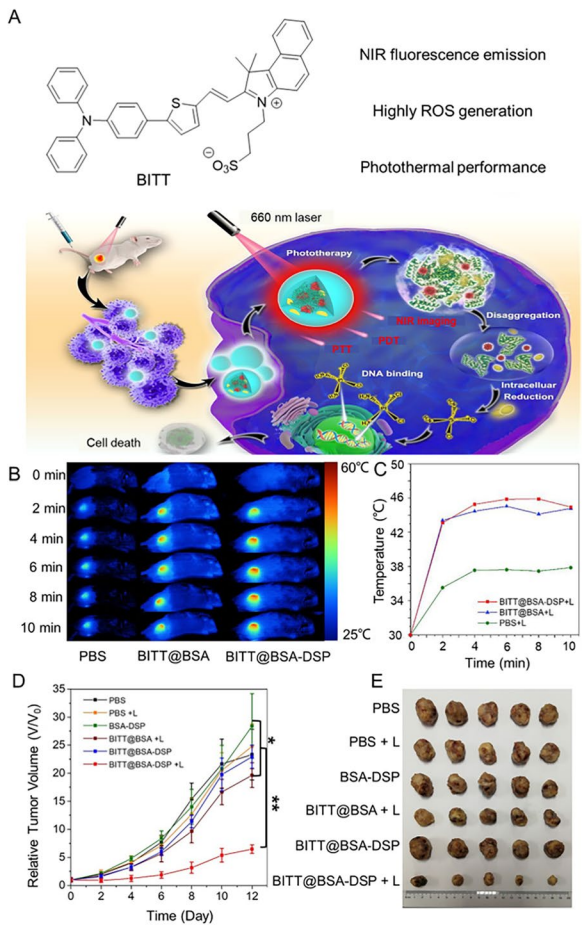

Fig. 15 **A** The structure of BITT and schematic illustrations and the treatment of bladder cancer by NIR FLI-guided photo-enhanced chemotherapy. **B** Infrared thermography of bladder tumor mice 6 h after intravenous injection with PBS, BITT@BSA NPs, and BITT@BSA–DSP NPs, followed by laser irradiation (660 nm, 0.3 W cm^{-2}, 10 min). **C** Average temperature of tumor regions. **D** Relative tumor volume growth curves of MB 49 tumor-bearing mice. **E** Representative tumor images of mice 12 days after different treatments. Reproduced with permission [232]. Copyright 2022, American Chemical Society

to chemotherapeutic drugs and even for effective treatment of drug resistance. In addition, sonodynamic therapy (SDT) is regarded as an effective method for cancer treatment due to its advantages of deep tumor penetration and high therapeutic efficacy. Guo et al. utilized a patient-derived MVs/AIEgen hybrid system (AMVs) for personalized SDT in a patient-derived xenograft (PDX) model of bladder cancer [233]. Impressive AMVs on PDX models displayed excellent tumor targeting capability and effective personalized SDT therapy.

In recent years, targeting molecules against bladder cancer has also been one of the focus of researchers. He et al. encapsulated AIE molecules with PEG and modified them with RGD on the surface to prepare a dual-function TPE-red-PEG-RGD nanoparticles that could be applied to target bladder cancer and image-guided PDT in vivo [234]. A combination of passive and active targeting was used to ensure the therapeutic effect, and targeted imaging in tumor regions and high anti-tumor efficacy could be achieved at a reasonable low dose (10 mg kg^{-1}). Besides, the combination of inorganic nanomaterials and AIE-PSs shows great potential to enhance the efficiency of PDT. They also modified nanographene oxides (NGO) with PEG chains and attempted to evaluate in vitro and in vivo PDT effects using NGP coated AIE nanoparticles (NGP-TPEred) [235]. PDT was evaluated using the UMUC3 (human bladder cancer cell line) tumor xenograft model. Tumor growth was immediately completely inhibited with the presence of NGP-TPEred nanoparticles and 450 nm laser irradiation, showing a significant difference compared to the other three groups. This shows the potential for NGP-TPEred nanoparticles to be used in PDT of bladder cancer.

PDT plays a particularly crucial role in cancer treatment. However, PDT remains poor due to the insufficient production of PS by ROS and the aggravation of hypoxia in the tumor microenvironment. To solve this problem, Guo et al. used the previously reported TFM as a ROS producer, together with the oxygen regulator doxycycline (DOXY), both of which are encapsulated into the NPs (D–P–T–D NPs), by utilizing powerful PDT in the oxygen-enriched tumor microenvironment and inhibiting tumor migration via regulating hypoxic-related pathways to defeat tumors [236]. Specifically, D–P–T–D NPs act on the tumor site by an EPR effect, and TFM is released from the NPs to produce powerful ROS with a 650 nm laser irradiation. With the introduction of DOXY, mitochondrial respiration was suppressed to overcome hypoxia by reducing endogenous oxygen consumption, further enhancing the efficacy of TFM-mediated PDT. Subsequent in vivo experiments verified that D–P–T–D NPs accumulated in tumor tissues through EPR effect, and reached a maximum accumulation in tumor tissues 4 h after injection to meet the therapeutic needs. In addition, D–P–T–D NPs exhibited excellent tumor killing effect under 650 nm laser irradiation (0.2 W, 5 min). Notably, there was almost no tumor growth in the D–P–T–D + Laser group during treatment, and more importantly, D–P–T–D NPs can inhibit tumor migration after PDT, thus improving the PDT effect. In short, the novel D–P–T–D NPs combined the optimized PDT effect and the inhibitory effect of tumor migration after PDT, suggesting a potent antitumor effect in the treatment of advanced bladder cancer.

Cholangiocarcinoma

Cholangiocarcinoma (CCA) is a malignant tumor originating in the extrahepatic bile duct from the hilar region to the lower common bile duct [237]. The incidence of CCA has increased significantly in the past few decades [238]. Surgical resection as the primary treatment for early cases is a good candidate for treatment of all subtypes of CCA [239]. However, the onset of CCA is insidious and the early symptoms are not obvious, so most patients are diagnosed at an advanced stage, which leads to the easy loss of the opportunity of surgical resection [240]. CCA is not sensitive to radiotherapy or chemotherapy in most cases, including gemcitabine and cisplatin chemotherapy, resulting in unsatisfactory efficacy and poor prognosis [241]. In order to improve the long-term survival probability of CCA patients, it is urgent to develop alternative treatment strategies in addition to surgical treatment [242, 243]. Since the first successful case of PDT in unresectable CCA was revealed, many clinical trials have indicated that PDT combined with biliary decompression can improve survival and post-treatment quality of life for CCA patients over the years [244–246].

Most patients with extrahepatic CCA are diagnosed as advanced stage and therefore cannot undergo timely curative surgical resection [247]. PDT is a highly effective ablative method of cancer cells, and has emerged as an alternative treatment strategy to increase the probability of long-term survival in patients with unresectable extrahepatic CCA. In order to achieve the broad application value of AIE materials in clinical diagnosis and treatment of CCA, Zheng and Liu et al. collaborated to develop an ideal PS (TTD) with long absorption wavelength to ensure the effect of photodynamic therapy on CCA [248]. As shown in Fig. 16, targeted delivery of NPs has been used to improve material enrichment at the tumor, so they take advantage of TTD to fabricate organic AIE dots with surface modification cRGD for image-guided PDT. Specifically, specific interaction between integrin $\alpha_v\beta_3$ and cRGD on T-TTD dots promoted the site to target tumor cells. To prove the above idea, the uptake of T-TTD dots in different cell lines, including QBC939 cells overexpressing $\alpha_v\beta_3$, normal L-O2 and HK-2 cells has been studied by CLSM and flow cytometry. All the experimental results were sufficient to prove that the integrin $\alpha_v\beta_3$ receptor-mediated endocytosis promoted the uptake of T-TTD dots. Next, synthetic T-TTD dots were injected into tumor-bearing mice to further evaluate the treatment effect of T-TTD dots-mediated by PDT in vivo, which could accumulate into tumor interstitial fluid through enhanced permeability and EPR effects. Tumor-bearing mice were divided into four groups, one of which was injected with T-TTD dots followed by laser irradiation (530 nm, 250 mW cm^{-2}), the tumor size decreased significantly, in contrast, tumors in the other three groups grew rapidly, including the group of saline injection only via the tail vein, the group of saline

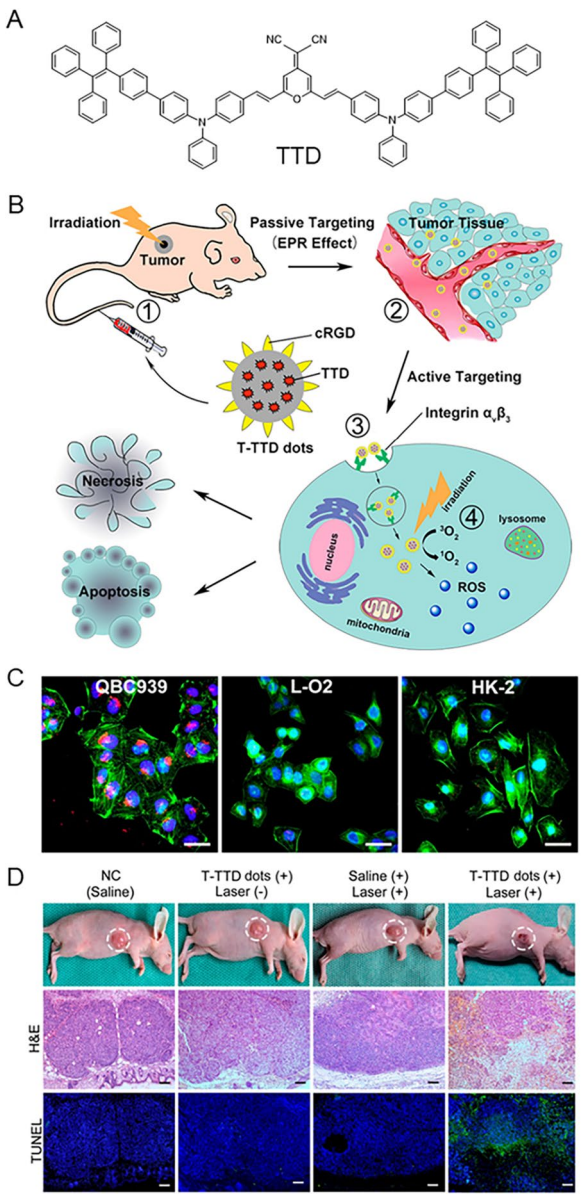

Fig. 16 **A** The structure of T-TTD. **B** Schematic illustration of T-TTD dots-mediated PDT in a human cholangiocarcinoma xenograft mouse model. **C** Fluorescent images of different cells after incubation with T-TTD dots for 4 h. Red fluorescence: T-TTD dots. Blue fluorescence: nuclei. Green fluorescence: cytoskeleton. Scale bars: 50 μm. **D** Photograph of a xenograft tumor 3 days after different treatments (white circles). H&E staining for pathological changes and TUNEL staining for apoptosis (green) in tumor sections. Scale:100 μm. Reproduced with permission [248]. Copyright 2017, American Chemical Society

injection followed by laser irradiation (530 nm, 250 mW cm^{-2}) and T-TTD dots injection without laser irradiation. These results suggest that T-TTD dots-mediated PDT is an effective and desirable treatment for CCA ablation. This makes AIE materials more promising for translational studies in the diagnosis and treatment of CCA in the future.

Study confirms that it is feasible to effectively ablate extrahepatic CCA cells through mitochondrial injury pathway. Li and Gao et al. are committed to developing PSs for PDT of CCA [249]. A mitochondrial anchored PS, TTVPHE, developed to effectively ablate extracellular CCA cells through mitochondrial injury pathway. When the irradiation time was extended to 15 min or the concentration of TTVPHE was increased to 7 mM, the extrahepatic CCA QBC939 cells viability was almost zero, indicating that TTVPHE had sufficient ability to kill cells and lay a foundation for tumor elimination in vivo.

Summary and outlook

PDT, as a novel non-invasive treatment method, has attracted extensive attention in biomedical applications. PS is one of the essential components of PDT, so its ROS production level directly determines the effect of PDT. It also has the advantage of fluorescence to combine optical imaging with PDT. This article reviews the current strategies of PDT in various tumors and guidelines for the development of high-efficiency AIE PSs. However, there are still many limitations in the design of efficient AIE PSs, and the PDT strategies based on AIE-PSs are still in their infancy, which requires continuous efforts to be applied in clinical practice. Here, we present some of the challenges of AIE PSs in tumor PDT treatment, and propose important research directions that require joint efforts.

1. The efficient activation of PSs by light sources that can penetrate deep into biological tissues plays an important role in optical PDT. However, the excitation peaks of most AIE PSs are the same as those of clinically approved PSs (*e.g.*, porphyrins and their derivatives), usually in the visible light range, resulting in shallow tissue penetration, which seriously impede their clinical application. Near infrared AIE PSs with highly ROS generation capability is developed to improve tissue penetration depth, such as two-photon photosensitizer. The emission wavelength of some PSs is covered by the background fluorescence of organisms, which is an urgent problem to be solved. So far, the reported AIE-PSs usually show emission peaks in the range of 600–700 nm, leading to problems such as low tissue imaging sensitivity. Therefore, highly efficient AIE-PSs with long-wavelength absorption and emission are highly desirable to advance improve the treatment accuracy and achieve visualized phototheranostics of cancer.
2. To overcome the toxicity and lack of specificity of photosensitizer and improve its bioavailability is always a problem to be solved. Nanomaterials have been widely modified to treat cancer. Although the number of studies has been increasing, the approved nanodrugs have not increased much in recent years. In order to better improve clinical transformation, further research is needed for targeted delivery of nanocarriers to reduce toxicity, enhance permeability and retention and avoid immune system clearance.
3. The cytotoxicity mechanism of PDT is different from the ones of chemotherapy, radiation therapy, immunotherapy and so on, so it presents unique advantages in treatment. PDT effects may be at least partially localized to the tumor, leading to cell death within tumors and reducing damage to normal cells. Moreover, PDT uses non-ionizing radiation in most cases, potentially promoting treated volume healing after treatment. To our pleasure, PDT can be used as many times as the clinician requires, which is not possible with currently available treatments such as surgery, chemotherapy, and radiation. In particular, PDT unique therapeutic mechanisms can inhibit drug resistance pathways and re-sensitize resistant cells to standard therapies. Despite the great potential of PDT, its application to deep-seated cancers and metastases remains challenging. It is mainly manifested in limited light penetration depth, non-ideal PSs, and complicated implementations in the clinic. Single PDT has inevitable drawbacks, so combining other therapies to effectively treat tumors is one of the desirable strategies. These therapies mainly include surgical treatment, chemotherapy, immunotherapy, radiotherapy, protein therapy, gene therapy and so on. Meanwhile, the synergistic effect of AIE PSs combined multiple treatments can be further enhanced via developing the functional design of material system.
4. Accurate and sensitive diagnosis and visual guidance are considered necessary to achieve accurate and efficient PDT. Conventional single-mode imaging methods have their own inherent defects. Fortunately, multi-mode imaging can complement each other to achieve the desired goal. Multifunctional phototherapy materials were exploited undoubtedly of great value for cancer treatment.
5. PDT is based on the phototoxicity of PSs after irradiation. However, most clinically approved PSs will be widely distributed in normal tissues, particularly in the skin, where they can produce phototoxicity with

serious side effects on exposure to light. As a result, the patients have to stay in a dark room for hours or even weeks during or after a PDT. AIE PSs designed to be sensitized in specific environments or conditions has been identified as a simple and effective way to liberate patients, which deserves further study.

At present, PDT has revealed unique advantages especially in the field of malignant tumors and skin diseases, especially in lung cancer, prostate cancer and skin tumor. The basic research and clinical application of PDT are in an active development trend. With the development of PSs from the first to the third generation, PDT has correspondingly more favorable properties, which can be better used in clinical trials. In this article, we put forward the advantages, limitations and future development direction of PDT based on AIE PSs in the field of tumor therapy. Encouragingly, there have been systemic and multifaceted demonstration using AIEgens for an optical imaging-guided surgical operation from small animals (mice and rabbits) to the typical non-human primate animal model (rhesus macaque). Although AIE PSs are still in their infancy for PDT of cancer, people have been making efforts and innovations in the mechanism of action and application in cancer treatment. The application limitations of PDT mentioned above are urgent problems for us to solve in the future. We hope to pay attention to current research hotspots and promote the further development of AIE PSs design, so that it can give full play to its advantages in clinical application.

Abbreviations

PDT: Photodynamic therapy; PSs: Photosensitizers; ACQ: Aggregation-caused quenching; ROS: Reactive oxygen species; AIE: Aggregation-induced emission; FDA: Food and Drug Administration; HPD: Porfimer sodium (Photofrin); ALA: 5-Aminolevulinic acid; mTHPC: Temoporfin (Foscan); AIEgens: AIE luminogens; LAPTM4B: Lysosomal protein transmembrane 4 beta; PTT: Photothermal therapy; S_0: The ground state; S_n: Higher-energy orbitals; S_1: The lowest singlet excited state; IC: Internal conversion; ISC: Intersystem crossover; ΔE_{ST}: The energy gap between excited S_1 and T_1 states; RIM: Restricted intermolecular motion; D: Electron donor; A: Electron acceptor; HOMO: The highest occupied molecular orbital; LUMO: The lowest unoccupied molecular orbital; TPE: Tetraphenylethylene; BT: 2,1,3-Benzothiadiazole; TCF: 2-Dicyanomethylene-3-cyano-4,5,5-trimethyl-2,5-dihydrofuran; C = O: Carbonyl group; –CN: Cyanide group; SOC: Spin–orbit coupling; TPA: Triphenylamine; RB: Rose Bengal; ABDA: 9,10-Anthracenediyl-bis(methylene)dimalonic acid; SOSG: Singlet Oxygen Sensor Green; PQ: 9,10-Phenanthrenequinone; AI-ISC: Aggregation-induced intersystem crossover; FA: Folic acid; PEG: Polyethylene glycol; PICAL: Photoimmune-regulating-liposome; BPD: Benzoporphyrin acid A; EGFR: Epidermal growth factor receptor; PPL: Preformed Plain Liposome; MPD: 1,2-Distearoyl-sn-glycero-3-phosphoethanolamine-N-[maleimide(polyethylene glycol)-2000]; R: Arginine; ER: Endoplasmic reticulum; ICD: Immunogenic cell death; hrHPV: High-risk human papillomavirus; CIN: Cervical intraepithelial neoplasia; HDACs: Histone deacetylases; GBM: Glioblastoma multiform; MDR: Multidrug resistance; BBB: Blood–brain barrier; BTB: Blood-tumor barrier; ApoE: Apolipoprotein E peptide; NIR-IIb: Near-infrared IIb; NK: Natural killer cells; MM: Malignant melanoma; NMSC: Non-melanoma skin cancer; CMM: Cutaneous malignant melanoma; NPs: Nanoparticles; BCC: Basal cell carcinoma; SCC: Squamous cell carcinoma; NSCLC: Non-small cell lung cancer; LDLR: Low-density lipoprotein receptors; LDL: Low-density lipoprotein; cis-Pt: Cisplatin; MCTSs: Multicellular tumor spheroids; Pt: Platinum; TPP: Triphenylphosphorus; FLI: Fluorescence imaging; PAI: Photoacoustic imaging; PTI: Photothermal imaging; HER2: Human epidermal growth factor receptor 2; CRC: Colorectal cancer; gFOBT: Guaiac fecal occult blood test; FIT: Fecal immunochemical test; FS: Flexible sigmoidoscopy; OC: Optical colonoscopy; GSH: Glutathione; CRPC: Castration of resistant prostate cancer; BLI: Bioluminescence imaging; PSMA: Prostate-specific membrane antigen; HCC: Hepatocellular carcinoma; BCLC: Barcelona Clinic Liver Cancer; TACE: Transarterial chemoembolization; TARE: Transarterial radioembolization; EpCAM: Epithelial cell adhesion molecule; MSHN: Mesoporous silica hollow nanospheres; NAC: Neoadjuvant chemotherapy; PECC: Photoenhanced cancer chemotherapy; SDT: Sonodynamic therapy; PDX: Patient-derived xenograft; NGO: Nanographene oxides; DOXY: Doxycycline; CCA: Cholangiocarcinoma; CLSM: Confocal laser scanning microscopy.

Acknowledgements

Not applicable.

Author contributions

The literature search and data analysis were performed by ZM and HX. The first draft of the manuscript was written by ZM, BC, XD and TW. The draft of the manuscript was revised by LY, XL, FX and JD, and all authors commented on previous versions of the manuscript. All authors read and approved the final manuscript.

Funding

This work was supported by the National Key R&D Program of China (2020YFA0211200), National Natural Science Foundation of China (22090050, 21974128, 21874121 and 22104040), the Natural Science Foundation of Hubei Province (2019CFA043 and 2020CFA037).

Availability of data and materials

Not applicable.

Declarations

Ethics approval and consent to participate

Not applicable.

Consent for publication

Not applicable.

Competing interests

The authors declare that they have no known competing financial interests or personal relationships that could have appeared to influence the work reported in this paper.

Author details

[1]State Key Laboratory of Biogeology and Environmental Geology, Faculty of Materials Science and Chemistry, China University of Geosciences, Wuhan 430074, China. [2]Institute of Pathology, Tongji Hospital, Tongji Medical College, Huazhong University of Science and Technology, Wuhan 430034, China. [3]Department of Obstetrics and Gynecology, Tongji Hospital, Tongji Medical College, Huazhong University of Science and Technology, Wuhan 430034, China.

Received: 30 May 2022 Accepted: 8 July 2022
Published online: 26 July 2022

References

1. Sung H, Ferlay J, Siegel RL, Laversanne M, Soerjomataram I, Jemal A, Bray F. Global cancer statistics 2020: GLOBOCAN estimates of incidence and mortality worldwide for 36 cancers in 185 countries. CA Cancer J Clin. 2021;71:209–49.
2. Bray F, Laversanne M, Weiderpass E, Soerjomataram I. The ever-increasing importance of cancer as a leading cause of premature death worldwide. Cancer. 2021;127:3029–30.

3. Xue T, Shen J, Shao K, Wang W, Wu B, He Y. Strategies for tumor hypoxia imaging based on aggregation-induced emission fluorogens. Chem Eur J. 2020;26:2521–8.
4. Li X, Lovell JF, Yoon J, Chen X. Clinical development and potential of photothermal and photodynamic therapies for cancer. Nat Rev Clin Oncol. 2020;17:657–74.
5. Correia JH, Rodrigues JA, Pimenta S, Dong T, Yang Z. Photodynamic therapy review: principles, photosensitizers, applications, and future directions. Pharmaceutics. 2021;13:1332.
6. Chen H, Wan Y, Cui X, Li S, Lee CS. Recent advances in hypoxia-overcoming strategy of aggregation-induced emission photosensitizers for efficient photodynamic therapy. Adv Healthc Mater. 2021;10:2101607.
7. Shen L, Zhou T, Fan Y, Chang X, Wang Y, Sun J, Xing L, Jiang H. Recent progress in tumor photodynamic immunotherapy. Chin Chem Lett. 2020;31:1709–16.
8. Jiang N, Zhou Z, Xiong W, Chen J, Shen J, Li R, Ye R. Tumor microenvironment triggered local oxygen generation and photosensitizer release from manganese dioxide mineralized albumin-ICG nanocomplex to amplify photodynamic immunotherapy efficacy. Chin Chem Lett. 2021;32:3948–53.
9. Daniell MD, Hill JS. A history of photodynamic therapy. Aust N Z J Surg. 1991;61:340–8.
10. Fan W, Huang P, Chen X. Overcoming the Achilles' heel of photodynamic therapy. Chem Soc Rev. 2016;45:6488–519.
11. Lu K, He C, Lin W. A Chlorin-based nanoscale metal–organic framework for photodynamic therapy of colon cancers. J Am Chem Soc. 2015;137:7600–3.
12. Wu L, Sun Y, Sugimoto K, Luo Z, Ishigaki Y, Pu K, Suzuki T, Chen HY, Ye D. Engineering of electrochromic materials as activatable probes for molecular imaging and photodynamic therapy. J Am Chem Soc. 2018;140:16340–52.
13. Adimoolam MG, Vijayalakshmi A, Nalam MR, Sunkara MV. Chlorin e6 loaded lactoferrin nanoparticles for enhanced photodynamic therapy. J Mater Chem B. 2017;5:9189–96.
14. Udartseva OO, Zhidkova OV, Ezdakova MI, Ogneva IV, Andreeva ER, Buravkova LB, Gollnick SO. Low-dose photodynamic therapy promotes angiogenic potential and increases immunogenicity of human mesenchymal stromal cells. J Photochem Photobiol B. 2019;199: 111596.
15. Dharmaraja AT. Role of reactive oxygen species (ROS) in therapeutics and drug resistance in cancer and bacteria. J Med Chem. 2017;60:3221–40.
16. Gunduz H, Kolemen S, Akkaya EU. Singlet oxygen probes: diversity in signal generation mechanisms yields a larger color palette. Coord Chem Rev. 2021;429: 213641.
17. Sadzuka Y, Tokutomi K, Iwasaki F, Sugiyama I, Hirano T, Konno H, Oku N, Sonobe T. The phototoxicity of photofrin was enhanced by PEGylated liposome in vitro. Cancer Lett. 2006;241:42–8.
18. Wu J, Lin Y, Li H, Jin Q, Ji J. Zwitterionic stealth peptide-capped 5-aminolevulinic acid prodrug nanoparticles for targeted photodynamic therapy. J Colloid Interface Sci. 2017;485:251–9.
19. Li K, Dong W, Miao Y, Liu Q, Qiu L, Lin J. Dual-targeted 5-aminolevulinic acid derivatives with glutathione depletion function for enhanced photodynamic therapy. J Photochem Photobiol B. 2021;215: 112107.
20. Haimov-Talmoud E, Harel Y, Schori H, Motiei M, Atkins A, Popovtzer R, Lellouche JP, Shefi O. Magnetic targeting of mTHPC to improve the selectivity and efficiency of photodynamic therapy. ACS Appl Mater Interfaces. 2019;11:45368–80.
21. Pereira SP, Ayaru L, Hatfield ARW, Rogowska A, Bown S. Photodynamic therapy (PDT) of malignant biliary strictures using meso-tetrahydroxyphenylchlorin (mTHPC). J Clin Oncol. 2005;23:4176–4176.
22. Vigneswaran K, Boyd NH, Oh SY, Lallani S, Boucher A, Neill SG, Olson JJ, Read RD. YAP/TAZ transcriptional coactivators create therapeutic vulnerability to verteporfin in EGFR-mutant glioblastoma. Clin Cancer Res. 2021;27:1553–69.
23. Price G, Anastasiadou M, Sudhir S, Bouras A, Tsankova N, Hadjipanayis C. ITVT-02. Elucidating the pleiotropic effects of verteporfin photodynamic therapy in preclinical glioblastoma models. NeuroOncology. 2021;23:vi228–vi228.
24. Zhao D, Tao W, Li S, Li L, Sun Y, Li G, Wang G, Wang Y, Lin B, Luo C, et al. Light-triggered dual-modality drug release of self-assembled prodrug-nanoparticles for synergistic photodynamic and hypoxia-activated therapy. Nanoscale Horiz. 2020;5:886–94.
25. Zhang Y, Ju J, Wang D, Yuan H, Hao L, Tan Y. Aggregation-induced emission for the visualization of the structure and properties of polymers. J Mater Chem C. 2021;9:11484–96.
26. Wan Q, Zhang R, Zhuang Z, Li Y, Huang Y, Wang Z, Zhang W, Hou J, Tang BZ. Molecular engineering to boost AIE-active free radical photogenerators and enable high-performance photodynamic therapy under hypoxia. Adv Funct Mater. 2020;30:2002057.
27. Zhao H, Xu J, Feng C, Ren J, Bao L, Zhao Y, Tao W, Zhao Y, Yang X. Tailoring aggregation extent of photosensitizers to boost phototherapy potency for eliciting systemic antitumor immunity. Adv Mater. 2022;34:2106390.
28. Luo J, Xie Z, Lam JWY, Cheng L, Chen H, Qiu C, Kwok HS, Zhan X, Liu Y, Zhu D, Tang BZ. Aggregation-induced emission of 1-methyl-1,2,3,4,5-pentaphenylsilole. Chem Commun. 2001;1740-1
29. Xue K, Dai Y, Zhao X, Zhang P, Ma F, Zhang D, Ji H, Wang X, Liang J, Qi Z. Boost highly efficient singlet oxygen generation and accelerate cancer cell apoptosis for photodynamic therapy by logically designed mitochondria targeted near-infrared AIEgens. Sens Actuators B. 2022;358: 131471.
30. Shi H, Pan X, Wang Y, Wang H, Liu W, Wang L, Chen Z. Restricting bond rotations by ring fusion: a novel molecular design strategy to improve photodynamic antibacterial efficacy of AIE photosensitizers. ACS Appl Mater Interfaces. 2022;14:17055–64.
31. Shi X, Sung SHP, Chau JHC, Li Y, Liu Z, Kwok RTK, Liu J, Xiao P, Zhang J, Liu B, et al. Killing G(+) or G(−) bacteria? the important role of molecular charge in AIE-active photosensitizers. Small Methods. 2020;4:2000046.
32. Zhu W, Kang M, Wu Q, Zhang Z, Wu Y, Li C, Li K, Wang L, Wang D, Tang BZ. Zwitterionic AIEgens: rational molecular design for NIR-II fluorescence imaging-guided synergistic phototherapy. Adv Funct Mater. 2021;31:2007026.
33. Gu X, Zhang X, Ma H, Jia S, Zhang P, Zhao Y, Liu Q, Wang J, Zheng X, Lam JWY, et al. Corannulene-incorporated AIE nanodots with highly suppressed nonradiative decay for boosted cancer phototheranostics in vivo. Adv Mater. 2018;30:1801065.
34. Tavakkoli Yaraki M, Wu M, Middha E, Wu W, Daqiqeh Rezaei S, Liu B, Tan YN. Gold nanostars-AIE theranostic nanodots with enhanced fluorescence and photosensitization towards effective image-guided photodynamic therapy. Nanomicro Lett. 2021;13:58.
35. Kang M, Kwok RTK, Wang J, Zhang H, Lam JWY, Li Y, Zhang P, Zou H, Gu X, Li F, Tang BZ. A multifunctional luminogen with aggregation-induced emission characteristics for selective imaging and photodynamic killing of both cancer cells and Gram-positive bacteria. J Mater Chem B. 2018;6:3894–903.
36. Alam P, Leung NLC, Zhang J, Kwok RTK, Lam JWY, Tang BZ. AIE-based luminescence probes for metal ion detection. Coord Chem Rev. 2021;429: 213693.
37. Wan H, Xu Q, Gu P, Li H, Chen D, Li N, He J, Lu J. AIE-based fluorescent sensors for low concentration toxic ion detection in water. J Hazard Mater. 2021;403: 123656.
38. Zhang Z, Kwok RTK, Yu Y, Tang BZ, Ng KM. Sensitive and specific detection of L-lactate using an AIE-active fluorophore. ACS Appl Mater Interfaces. 2017;9:38153–8.
39. Yan N, Hu Y, Tang BZ, Wang W-X. Real-time 3D framework tracing of extracellular polymeric substances by an AIE-active nanoprobe. ACS Sensors. 2021;6:4206–16.
40. Wang Y, Zhang Y, Wang J, Liang X-J. Aggregation-induced emission (AIE) fluorophores as imaging tools to trace the biological fate of nano-based drug delivery systems. Adv Drug Deliv Rev. 2019;143:161–76.
41. Jang SE, Qiu L, Cai X, Lee JWL, Zhang W, Tan E-K, Liu B, Zeng L. Aggregation-induced emission (AIE) nanoparticles labeled human embryonic stem cells (hESCs)-derived neurons for transplantation. Biomaterials. 2021;271: 120747.
42. Li WJ, Zhang YP, Wang YC, Ma Y, Wang DY, Li H, Ye XY, Yin F, Li ZG. Nucleic acids induced peptide-based AIE nanoparticles for fast cell imaging. Chin Chem Lett. 2021;32:1571–4.

43. Dai J, Xue H, Chen D, Lou X, Xia F, Wang S. Aggregation-induced emission luminogens for assisted cancer surgery. Coord Chem Rev. 2022;464: 214552.
44. Dai J, Dong X, Wang Q, Lou X, Xia F, Wang S. PEG-polymer encapsulated aggregation-induced emission nanoparticles for tumor theranostics. Adv Healthc Mater. 2021;10:2101036.
45. Cheng Y, Dai J, Sun C, Liu R, Zhai T, Lou X, Xia F. An intracellular H_2O_2-responsive AIEgen for the peroxidase-mediated selective imaging and inhibition of inflammatory cells. Angew Chem Int Ed. 2018;57:3123–7.
46. Li J, Meng Z, Zhuang Z, Wang B, Dai J, Feng G, Lou X, Xia F, Zhao Z, Tang BZ. Effective therapy of drug-resistant bacterial infection by killing planktonic bacteria and destructing biofilms with cationic photosensitizer based on phosphindole oxide. Small. 2022;18:2200743.
47. Liu J, Liu X, Wu M, Qi G, Liu B. Engineering living mitochondria with AIE photosensitizer for synergistic cancer cell ablation. Nano Lett. 2020;20:7438–45.
48. Liu Z, Zou H, Zhao Z, Zhang P, Shan GG, Kwok RTK, Lam JWY, Zheng L, Tang BZ. Tuning organelle specificity and photodynamic therapy efficiency by molecular function design. ACS Nano. 2019;13:11283–93.
49. Shi L, Hu F, Duan Y, Wu W, Dong J, Meng X, Zhu X, Liu B. Hybrid nanospheres to overcome hypoxia and intrinsic oxidative resistance for enhanced photodynamic therapy. ACS Nano. 2020;14:2183–90.
50. Wu W, Mao D, Xu S, Panahandeh-Fard M, Duan Y, Hu F, Kong D, Liu B. Precise molecular engineering of photosensitizers with aggregation-induced emission over 800 nm for photodynamic therapy. Adv Funct Mater. 2019;29:1901791.
51. Yuan Y, Feng G, Qin W, Tang BZ, Liu B. Targeted and image-guided photodynamic cancer therapy based on organic nanoparticles with aggregation-induced emission characteristics. Chem Commun. 2014;50:8757–60.
52. Hu F, Huang Y, Zhang G, Zhao R, Yang H, Zhang D. Targeted bioimaging and photodynamic therapy of cancer cells with an activatable red fluorescent bioprobe. Anal Chem. 2014;86:7987–95.
53. De Las HE, Sagristá ML, Agut M, Nonell S. Photosensitive EGFR-targeted nanocarriers for combined photodynamic and local chemotherapy. Pharmaceutics. 2022;14:405.
54. Yang G, Tian J, Chen C, Jiang D, Xue Y, Wang C, Gao Y, Zhang W. An oxygen self-sufficient NIR-responsive nanosystem for enhanced PDT and chemotherapy against hypoxic tumors. Chem Sci. 2019;10:5766–72.
55. Wei D, Chen Y, Huang Y, Li P, Zhao Y, Zhang X, Wan J, Yin X, Liu T, Yin J, et al. NIR-light triggered dual-cascade targeting core-shell nanoparticles enhanced photodynamic therapy and immunotherapy. Nano Today. 2021;41: 101288.
56. Dai J, Dong X, Liu R, Chen B, Dong X, Wang Q, Hu J-J, Xia F, Lou X. A peptide-AIEgen nanocomposite mediated whole cancer immunity cycle-cascade amplification for improved immunotherapy of tumor. Biomaterials. 2022;285: 121528.
57. Xu J, Zheng Q, Cheng X, Hu S, Zhang C, Zhou X, Sun P, Wang W, Su Z, Zou T, et al. Chemo-photodynamic therapy with light-triggered disassembly of theranostic nanoplatform in combination with checkpoint blockade for immunotherapy of hepatocellular carcinoma. J Nanobiotechnol. 2021;19:355.
58. Liu J, Hu F, Wu M, Tian L, Gong F, Zhong X, Chen M, Liu Z, Liu B. Bioorthogonal coordination polymer nanoparticles with aggregation-induced emission for deep tumor-penetrating radio- and radiodynamic therapy. Adv Mater. 2021;33:2007888.
59. Dai J, Hu J-J, Dong X, Chen B, Dong X, Liu R, Xia F, Lou X. Deep down-regulation of PD-L1 by caged peptide-conjugated AIEgen/miR-140 nanoparticles for enhanced immunotherapy. Angew Chem Int Ed. 2022;61: e202117798.
60. Van Straten D, Mashayekhi V, De Bruijn HS, Oliveira S, Robinson DJ. Oncologic photodynamic therapy: basic principles, current clinical status and future directions. Cancers. 2017;9:19.
61. Pham TC, Nguyen VN, Choi Y, Lee S, Yoon J. Recent strategies to develop innovative photosensitizers for enhanced photodynamic therapy. Chem Rev. 2021;121:13454–619.
62. Xu S, Yuan Y, Cai X, Zhang CJ, Hu F, Liang J, Zhang G, Zhang D, Liu B. Tuning the singlet-triplet energy gap: a unique approach to efficient photosensitizers with aggregation-induced emission (AIE) characteristics. Chem Sci. 2015;6:5824–30.
63. Chen H, Li S, Wu M, Huang Z, Lee CS, Liu B. Membrane-anchoring photosensitizer with aggregation-induced emission characteristics for combating multidrug-resistant bacteria. Angew Chem Int Ed. 2020;59:632–6.
64. Zha M, Yang G, Li Y, Zhang C, Li B, Li K. Recent advances in AIEgen-based photodynamic therapy and immunotherapy. Adv Healthc Mater. 2021;10:2101066.
65. Tu Y, Liu J, Zhang H, Peng Q, Lam JWY, Tang BZ. Restriction of access to the dark state: a new mechanistic model for heteroatom-containing AIE systems. Angew Chem Int Ed. 2019;58:14911–4.
66. Tu Y, Zhao Z, Lam JWY, Tang BZ. Mechanistic connotations of restriction of intramolecular motions (RIM). Natl Sci Rev. 2021;8:nwaa260.
67. Dai J, Wu X, Ding S, Lou X, Xia F, Wang S, Hong Y. Aggregation-induced emission photosensitizers: from molecular design to photodynamic therapy. J Med Chem. 2020;63:1996–2012.
68. Wu WB, Mao D, Xu SD, Kenry R, Hu F, Li XQ, Kong DL, Liu B. Polymerization-enhanced photosensitization. Chem. 2018;4:1937–51.
69. Chen Y, Ai W, Guo X, Li Y, Ma Y, Chen L, Zhang H, Wang T, Zhang X, Wang Z. Mitochondria-targeted polydopamine nanocomposite with AIE photosensitizer for image-guided photodynamic and photothermal tumor ablation. Small. 2019;15:1902352.
70. Li L, Yuan G, Qi Q, Lv C, Liang J, Li H, Cao L, Zhang X, Wang S, Cheng Y, He H. Synthesis of tetraphenylethene-based D-A conjugated molecules with near-infrared AIE features, and their application in photodynamic therapy. J Mater Chem B. 2022;10:3550–9.
71. Zhang F, Liu Y, Yang B, Wen G, Liu B. Near-infrared AIEgens for lipid droplets imaging in corpus adiposum or trachea of Locusta migratoria and its application in photodynamic therapy. Sens Actuators B. 2020;322: 128589.
72. Yang M, Deng J, Su H, Gu S, Zhang J, Zhong A, Wu F. Small organic molecule-based nanoparticles with red/near-infrared aggregation-induced emission for bioimaging and PDT/PTT synergistic therapy. Mate Chem Front. 2021;5:406–17.
73. Ding GY, Tong J, Gong JY, Wang Z, Su ZM, Liu L, Han X, Wang J, Zhang L, Wang X, et al. Molecular engineering to achieve AIE-active photosensitizer with NIR emission and rapid ROS generation efficiency. J Mater Chem B. 2022;10:5272-8.
74. Wang Z, Wang C, Gan Q, Cao Y, Yuan H, Hua D. Donor–acceptor-type conjugated polymer-based multicolored drug carriers with tunable aggregation-induced emission behavior for self-illuminating cancer therapy. ACS Appl Mater Interfaces. 2019;11:41853–61.
75. Gon M, Tanaka K, Chujo Y. A highly efficient near-infrared-emissive copolymer with a N═N double-bond π-conjugated system based on a fused azobenzene-boron complex. Angew Chem Int Ed. 2018;57:6546–51.
76. Khan IM, Niazi S, Iqbal Khan MK, Pasha I, Mohsin A, Haider J, Iqbal MW, Rehman A, Yue L, Wang Z. Recent advances and perspectives of aggregation-induced emission as an emerging platform for detection and bioimaging. TrAC Trends Anal Chem. 2019;119: 115637.
77. Yang Z, Zhang Z, Sun Y, Lei Z, Wang D, Ma H, Tang BZ. Incorporating spin-orbit coupling promoted functional group into an enhanced electron D-A system: a useful designing concept for fabricating efficient photosensitizer and imaging-guided photodynamic therapy. Biomaterials. 2021;275: 120934.
78. Li Y, Zhang R, Wan Q, Hu R, Ma Y, Wang Z, Hou J, Zhang W, Tang BZ. Trojan horse-like nano-AIE aggregates based on homologous targeting strategy and their photodynamic therapy in anticancer application. Adv Sci. 2021;8:2102561.
79. You X, Ma H, Wang Y, Zhang G, Peng Q, Liu L, Wang S, Zhang D. Pyridinium-substituted tetraphenylethylene entailing alkyne moiety: enhancement of photosensitizing efficiency and antimicrobial activity. Chem Asian J. 2017;12:1013–9.
80. Zhang L, Li Y, Che W, Zhu D, Li G, Xie Z, Song N, Liu S, Tang BZ, Liu X, et al. AIE multinuclear Ir(III) complexes for biocompatible organic nanoparticles with highly enhanced photodynamic performance. Adv Sci. 2019;6:1802050.
81. Cai X, Wang K-N, Ma W, Yang Y, Chen G, Fu H, Cui C, Yu Z, Wang X. Multifunctional AIE iridium (III) photosensitizer nanoparticles for two-photon-activated imaging and mitochondria targeting photodynamic therapy. J Nanobiotechnol. 2021;19:254.

82. Li X, Kwon N, Guo T, Liu Z, Yoon J. Innovative strategies for hypoxic-tumor photodynamic therapy. Angew Chem Int Ed. 2018;57:11522–31.
83. Kang M, Zhang Z, Xu W, Wen H, Zhu W, Wu Q, Wu H, Gong J, Wang Z, Wang D, Tang BZ. Good steel used in the blade: well-tailored type-I photosensitizers with aggregation-induced emission characteristics for precise nuclear targeting photodynamic therapy. Adv Sci. 2021;8:2100524.
84. Zhuang Z, Dai J, Yu M, Li J, Shen P, Hu R, Lou X, Zhao Z, Tang BZ. Type I photosensitizers based on phosphindole oxide for photodynamic therapy: apoptosis and autophagy induced by endoplasmic reticulum stress. Chem Sci. 2020;11:3405–17.
85. Guo J, Dai J, Peng X, Wang Q, Wang S, Lou X, Xia F, Zhao Z, Tang BZ. 9,10-Phenanthrenequinone: a promising kernel to develop multifunctional antitumor systems for efficient type I photodynamic and photothermal synergistic therapy. ACS Nano. 2021;15:20042–55.
86. Liu S, Wang B, Yu Y, Liu Y, Zhuang Z, Zhao Z, Feng G, Qin A, Tang BZ. Cationization-enhanced type I and type II ROS generation for photodynamic treatment of drug-resistant bacteria. ACS Nano. 2022;16:9130-41.
87. Yang G, Ni J-S, Li Y, Zha M, Tu Y, Li K. Acceptor engineering for optimized ROS generation facilitates reprogramming macrophages to M1 phenotype in photodynamic immunotherapy. Angew Chem Int Ed. 2021;60:5386–93.
88. Zhao X, Dai Y, Ma F, Misal S, Hasrat K, Zhu H, Qi Z. Molecular engineering to accelerate cancer cell discrimination and boost AIE-active type I photosensitizer for photodynamic therapy under hypoxia. Chem Eng J. 2021;410: 128133.
89. Liu Z, Wang Q, Qiu W, Lyu Y, Zhu Z, Zhao X, Zhu W-H. AIE-active luminogens as highly efficient free-radical ROS photogenerator for image-guided photodynamic therapy. Chem Sci. 2022;13:3599–608.
90. Hu R, Qin A, Tang BZ. AIE polymers: synthesis and applications. Prog Polym Sci. 2020;100: 101176.
91. Hu R, Leung NLC, Tang BZ. AIE macromolecules: syntheses, structures and functionalities. Chem Soc Rev. 2014;43:4494–562.
92. Qin A, Lam JWY, Tang BZ. Luminogenic polymers with aggregation-induced emission characteristics. Prog Polym Sci. 2012;37:182–209.
93. Liu S, Zhang H, Li Y, Liu J, Du L, Chen M, Kwok RTK, Lam JWY, Phillips DL, Tang BZ. Strategies to enhance the photosensitization: polymerization and the donor–acceptor even–odd effect. Angew Chem Int Ed. 2018;57:15189–93.
94. Xie H, Hu W, Zhang F, Zhao C, Peng T, Zhu C, Xu J. AIE-active polyelectrolyte based photosensitizers: the effects of structure on antibiotic-resistant bacterial sensing and killing and pollutant decomposition. J Mater Chem B. 2021;9:5309–17.
95. Wang Y, Sun Y, Ran J, Yang H, Xiao S, Yang J, Yang C, Wang H, Liu Y. Utilization of nonradiative excited-state dissipation for promoted phototheranostics based on an AIE-active type I ROS generator. ACS Appl Mater Interfaces. 2022;14:225–35.
96. Zhou Y, Jing S, Liu S, Shen X, Cai L, Zhu C, Zhao Y, Pang M. Double-activation of mitochondrial permeability transition pore opening via calcium overload and reactive oxygen species for cancer therapy. J Nanobiotechnol. 2022;20:188.
97. Dai J, Chen Z, Wang S, Xia F, Lou X. Erythrocyte membrane-camouflaged nanoparticles as effective and biocompatible platform: either autologous or allogeneic erythrocyte-derived. Mater Today Bio. 2022;15: 100279.
98. Dai J, Wu M, Wang Q, Ding S, Dong X, Xue L, Zhu Q, Zhou J, Xia F, Wang S, Hong Y. Red blood cell membrane-camouflaged nanoparticles loaded with AIEgen and Poly(I : C) for enhanced tumoral photodynamic-immunotherapy. Natl Sci Rev. 2021;8:39.
99. Yang J, Dai J, Wang Q, Cheng Y, Guo J, Zhao Z, Hong Y, Lou X, Xia F. Tumor-triggered disassembly of a multiple-agent-therapy probe for efficient cellular internalization. Angew Chem Int Ed. 2020;59:20405–10.
100. Zou J, Chen S, Li Y, Zeng L, Lian G, Li J, Chen S, Huang K, Chen Y. Nanoparticles modified by triple single chain antibodies for MRI examination and targeted therapy in pancreatic cancer. Nanoscale. 2020;12:4473–90.
101. Camardo A, Carney S, Ramamurthi A. Assessing the targeting and fate of cathepsin k antibody-modified nanoparticles in a rat abdominal aortic aneurysm model. Acta Biomater. 2020;112:225–33.
102. Wang L, Wang X, Yang F, Liu Y, Meng L, Pang Y, Zhang M, Chen F, Pan C, Lin S, et al. Systemic antiviral immunization by virus-mimicking nanoparticles-decorated erythrocytes. Nano Today. 2021;40: 101280.
103. Takahashi M, Yoshino T, Matsunaga T. Surface modification of magnetic nanoparticles using asparagines-serine polypeptide designed to control interactions with cell surfaces. Biomaterials. 2010;31:4952–7.
104. Sun C, Du K, Fang C, Bhattarai N, Veiseh O, Kievit F, Stephen Z, Lee D, Ellenbogen RG, Ratner B, Zhang M. PEG-mediated synthesis of highly dispersive multifunctional superparamagnetic nanoparticles: their physicochemical properties and function in vivo. ACS Nano. 2010;4:2402–10.
105. Wang S, Li K, Chen Y, Chen H, Ma M, Feng J, Zhao Q, Shi J. Biocompatible PEGylated MoS2 nanosheets: controllable bottom-up synthesis and highly efficient photothermal regression of tumor. Biomaterials. 2015;39:206–17.
106. Mao L, Huang H, Hu D, Ma H, Tian M, Zhang X, Wei Y. A near-infrared bioprobe with aggregation-induced emission feature for in vitro photodynamic therapy. Dyes Pigm. 2021;194: 109521.
107. Wen Q, Zhang Y, Li C, Ling S, Yang X, Chen G, Yang Y, Wang Q. NIR-II fluorescent self-assembled peptide nanochain for ultrasensitive detection of peritoneal metastasis. Angew Chem Int Ed. 2019;58:11001–6.
108. Tian C, Qian W, Shao X, Xie Z, Cheng X, Liu S, Cheng Q, Liu B, Wang X. Plasmonic nanoparticles with quantitatively controlled bioconjugation for photoacoustic imaging of live cancer cells. Adv Sci. 2016;3:1600237.
109. Wan G, Cheng Y, Song J, Chen Q, Chen B, Liu Y, Ji S, Chen H, Wang Y. Nucleus-targeting near-infrared nanoparticles based on TAT peptide-conjugated IR780 for photo-chemotherapy of breast cancer. Chem Eng J. 2020;380: 122458.
110. Li N, Sun Q, Yu Z, Gao X, Pan W, Wan X, Tang B. Nuclear-targeted photothermal therapy prevents cancer recurrence with near-infrared triggered copper sulfide nanoparticles. ACS Nano. 2018;12:5197–206.
111. Lee MX, Tan DSP. Weekly versus 3-weekly paclitaxel in combination with carboplatin in advanced ovarian cancer: which is the optimal adjuvant chemotherapy regimen? J Gynecol Oncol. 2018;29: e96.
112. Nimmagadda S, Penet MF. Ovarian cancer targeted theranostics. Front Oncol. 2020;9:1537.
113. Moufarrij S, Dandapani M, Arthofer E, Gomez S, Srivastava A, Lopez Acevedo M, Villagra A, Chiappinelli KB. Epigenetic therapy for ovarian cancer: promise and progress. Clin Epigenet. 2019;11:7.
114. Mir Y, Elrington SA, Hasan T. A new nanoconstruct for epidermal growth factor receptor-targeted photo-immunotherapy of ovarian cancer. Nanomedicine. 2013;9:1114–22.
115. Dai J, Li Y, Long Z, Jiang R, Zhuang Z, Wang Z, Zhao Z, Lou X, Xia F, Tang BZ. Efficient near-infrared photosensitizer with aggregation-induced emission for imaging-guided photodynamic therapy in multiple xenograft tumor models. ACS Nano. 2020;14:854–66.
116. Dai J, Cheng Y, Wu J, Wang Q, Wang W, Yang J, Zhao Z, Lou X, Xia F, Wang S, Tang BZ. Modular peptide probe for pre/intra/postoperative therapeutic to reduce recurrence in ovarian cancer. ACS Nano. 2020;14:14698–714.
117. Li X, Zhao Y, Zhang T, Xing D. Mitochondria-specific agents for photodynamic cancer therapy: a key determinant to boost the efficacy. Adv Healthc Mater. 2021;10:2001240.
118. Deng H, Zhou Z, Yang W, Lin LS, Wang S, Niu G, Song J, Chen X. Endoplasmic reticulum targeting to amplify immunogenic cell death for cancer immunotherapy. Nano Lett. 2020;20:1928–33.
119. Dyer O. Cervical cancer: deaths increase as HPV vaccine is underused, says WHO. BMJ. 2019;364: l580.
120. Lecavalier Barsoum M, Chaudary N, Han K, Koritzinsky M, Hill R, Milosevic M. Targeting the CXCL12/CXCR4 pathway and myeloid cells to improve radiation treatment of locally advanced cervical cancer. Int J Cancer. 2018;143:1017–28.
121. Inada NM, Buzzá HH, Leite MF, Kurachi C, Trujillo JR, de Castro CA, Carbinatto FM, Lombardi W, Bagnato VS. Long term effectiveness of photodynamic therapy for CIN treatment. Pharmaceuticals. 2019;12:107.
122. Hillemanns P, Petry KU, Soergel P, Collinet P, Ardaens K, Gallwas J, Luyten A, Dannecker C. Efficacy and safety of hexaminolevulinate photodynamic therapy in patients with low-grade cervical intraepithelial neoplasia. Lasers Surg Med. 2014;46:456–61.
123. Liu X-Y, Yang JB, Wu CY, Tang Q, Lu ZL, Lin L. [12]aneN_3-Conjugated AIEgens with two-photon imaging properties for synergistic gene/photodynamic therapy in vitro and in vivo. J Mater Chem B. 2022;10:945–57.

124. Tang F, Liu JY, Wu CY, Liang YX, Lu ZL, Ding AX, Xu MD. Two-photon near-infrared AIE luminogens as multifunctional gene carriers for cancer theranostics. ACS Appl Mater Interfaces. 2021;13:23384–95.
125. Zou H, Zhang J, Wu C, He B, Hu Y, Sung HHY, Kwok RTK, Lam JWY, Zheng L, Tang BZ. Making aggregation-induced emission luminogen more valuable by gold: enhancing anticancer efficacy by suppressing thioredoxin reductase activity. ACS Nano. 2021;15:9176–85.
126. Wen D, Zhang X, Ding L, Wen H, Liu W, Zhang C, Wang B, Li L, Diao H. Folic acid functionalized aggregation-induced emission nanoparticles for tumor cell targeted imaging and photodynamic therapy. RSC Adv. 2022;12:4484–9.
127. Jiang M, Kwok RTK, Li X, Gui C, Lam JWY, Qu J, Tang BZ. A simple mitochondrial targeting AIEgen for image-guided two-photon excited photodynamic therapy. J Mater Chem B. 2018;6:2557–65.
128. Wang KN, Liu LY, Mao D, Hou MX, Tan CP, Mao ZW, Liu B. A nuclear-targeted AIE photosensitizer for enzyme inhibition and photosensitization in cancer cell ablation. Angew Chem Int Ed. 2022;61: e202114600.
129. Zhang L, Che W, Yang Z, Liu X, Liu S, Xie Z, Zhu D, Su Z, Tang BZ, Bryce MR. Bright red aggregation-induced emission nanoparticles for multifunctional applications in cancer therapy. Chem Sci. 2020;11:2369–74.
130. Valvona CJ, Fillmore HL, Nunn PB, Pilkington GJ. The regulation and function of lactate dehydrogenase A: therapeutic potential in brain tumor. Brain Pathol. 2016;26:3–17.
131. Gutmann DH, Kettenmann H. Microglia/Brain macrophages as central drivers of brain tumor pathobiology. Neuron. 2019;104:442–9.
132. Ladomersky E, Scholtens DM, Kocherginsky M, Hibler EA, Bartom ET, Otto-Meyer S, Zhai L, Lauing KL, Choi J, Sosman JA, et al. The coincidence between increasing age, immunosuppression, and the incidence of patients with glioblastoma. Front Pharmacol. 2019;10:200.
133. Emran TB, Shahriar A, Mahmud AR, Rahman T, Abir MH, Siddiquee MF-R, Ahmed H, Rahman N, Nainu F, Wahyudin E, et al. Multidrug resistance in cancer: understanding molecular mechanisms, immunoprevention and therapeutic approaches. Front Oncol. 2022;12:891652.
134. Larsen AK, Escargueil AE, Skladanowski A. Resistance mechanisms associated with altered intracellular distribution of anticancer agents. Pharmacol Ther. 2000;85:217–29.
135. Wu Q, Yang Z, Nie Y, Shi Y, Fan D. Multi-drug resistance in cancer chemotherapeutics: mechanisms and lab approaches. Cancer Lett. 2014;347:159–66.
136. Zhao CY, Cheng R, Yang Z, Tian ZM. Nanotechnology for cancer therapy based on chemotherapy. Molecules. 2018;23:826.
137. Lee YT, Tan YJ, Oon CE. Molecular targeted therapy: treating cancer with specificity. Eur J Pharmacol. 2018;834:188–96.
138. Wilkes GM. Targeted therapy: attacking cancer with molecular and immunological targeted agents. Asia Pac J Clin Onco. 2018;5:137–55.
139. Cheng Z, Li M, Dey R, Chen Y. Nanomaterials for cancer therapy: current progress and perspectives. J Hematol Oncol. 2021;14:85.
140. Sheng Z, Guo B, Hu D, Xu S, Wu W, Liew WH, Yao K, Jiang J, Liu C, Zheng H, Liu B. Bright aggregation-induced-emission dots for targeted synergetic NIR-II fluorescence and NIR-I photoacoustic imaging of orthotopic brain tumors. Adv Mater. 2018;30:1800766.
141. Gao D, Li Y, Wu Y, Liu Y, Hu D, Liang S, Liao J, Pan M, Zhang P, Li K, et al. Albumin-consolidated AIEgens for boosting glioma and cerebrovascular NIR-II fluorescence imaging. ACS Appl Mater Interfaces. 2022. https://doi.org/10.1021/acsami.1c22700.
142. Luo D, Carter KA, Miranda D, Lovell JF. Chemophototherapy: an emerging treatment option for solid tumors. Adv Sci. 2017;4:1600106.
143. Lim C, Moon J, Sim T, Won WR, Lee ES, Youn YS, Oh KT. A nano-complex system to overcome antagonistic photo-chemo combination cancer therapy. J Control Release. 2019;295:164–73.
144. Li Y, Deng Y, Tian X, Ke H, Guo M, Zhu A, Yang T, Guo Z, Ge Z, Yang X, Chen H. Multipronged design of light-triggered nanoparticles to overcome cisplatin resistance for efficient ablation of resistant tumor. ACS Nano. 2015;9:9626–37.
145. Guo B, Wu M, Shi Q, Dai T, Xu S, Jiang J, Liu B. All-in-one molecular aggregation-induced emission theranostics: fluorescence image guided and mitochondria targeted chemo- and photodynamic cancer cell ablation. Chem Mater. 2020;32:4681–91.
146. Fortin D. The blood-brain barrier: its influence in the treatment of brain tumors metastases. Curr Cancer Drug Targets. 2012;12:247–59.
147. Tang J, Wang Q, Yu Q, Qiu Y, Mei L, Wan D, Wang X, Li M, He Q. A stabilized retro-inverso peptide ligand of transferrin receptor for enhanced liposome-based hepatocellular carcinoma-targeted drug delivery. Acta Biomater. 2019;83:379–89.
148. Kuang Y, An S, Guo Y, Huang S, Shao K, Liu Y, Li J, Ma H, Jiang C. T7 peptide-functionalized nanoparticles utilizing RNA interference for glioma dual targeting. Int J Pharm. 2013;454:11–20.
149. Hu K, Zhou D, Rao L, Wang P, Xiang C, Chen F. A multifunctional AIE nanoprobe as a drug delivery bioimaging and cancer treatment system. Front Bioeng Biotechnol. 2021;9:766470.
150. Jiang Y, Zhang J, Meng F, Zhong Z. Apolipoprotein E peptide-directed chimeric polymersomes mediate an ultrahigh-efficiency targeted protein therapy for glioblastoma. ACS Nano. 2018;12:11070–9.
151. Wang J, Liu Y, Morsch M, Lu Y, Shangguan P, Han L, Wang Z, Chen X, Song C, Liu S, et al. Brain-targeted aggregation-induced-emission nanoparticles with near-infrared imaging at 1550 nm boosts orthotopic glioblastoma theranostics. Adv Mater. 2022;34:2106082.
152. Deng G, Peng X, Sun Z, Zheng W, Yu J, Du L, Chen H, Gong P, Zhang P, Cai L, Tang BZ. Natural-killer-cell-inspired nanorobots with aggregation-induced emission characteristics for near-infrared-II fluorescence-guided glioma theranostics. ACS Nano. 2020;14:11452–62.
153. Whiteman DC, Green AC, Olsen CM. The growing burden of invasive melanoma: projections of incidence rates and numbers of new cases in six susceptible populations through 2031. J Invest Dermatol. 2016;136:1161–71.
154. de Vries E, Willem CJ. Cutaneous malignant melanoma in Europe. Eur J Cancer. 2004;40:2355–66.
155. Blume-Peytavi U. 9th skin academy symposium: building bridges in dermatology chair's introduction. Dermatol Ther. 2017;7:1–3.
156. Juszczak AM, Wöelfle U, Končić MZ, Tomczyk M. Skin cancer, including related pathways and therapy and the role of luteolin derivatives as potential therapeutics. Med Res Rev. 2022;42:1423-62.
157. Su MY, Fisher DE. Immunotherapy in the precision medicine era: melanoma and beyond. PLoS Med. 2016;13: e1002196.
158. Guadagnolo BA, Zagars GK. Adjuvant radiation therapy for high-risk nodal metastases from cutaneous melanoma. Lancet Oncol. 2009;10:409–16.
159. Zheng Z, Liu H, Zhai S, Zhang H, Shan G, Kwok RTK, Ma C, Sung HHY, Williams ID, Lam JWY, et al. Highly efficient singlet oxygen generation, two-photon photodynamic therapy and melanoma ablation by rationally designed mitochondria-specific near-infrared AIEgens. Chem Sci. 2020;11:2494–503.
160. Li Y, Tang R, Liu X, Gong J, Zhao Z, Sheng Z, Zhang J, Li X, Niu G, Kwok RTK, et al. Bright aggregation-induced emission nanoparticles for two-photon imaging and localized compound therapy of cancers. ACS Nano. 2020;14:16840–53.
161. Kashyap MP, Sinha R, Mukhtar MS, Athar M. Epigenetic regulation in the pathogenesis of non-melanoma skin cancer. Semin Cancer Biol. 2020;83:36-56.
162. Wan J, Dai H, Zhang X, Liu S, Lin Y, Somani AK, Xie J, Han J. Distinct transcriptomic landscapes of cutaneous basal cell carcinomas and squamous cell carcinomas. Genes Dis. 2021;8:181–92.
163. Wang J, Zhu X, Zhang J, Wang H, Liu G, Bu Y, Yu J, Tian Y, Zhou H. AIE-based theranostic agent: in situ tracking mitophagy prior to late apoptosis to guide the photodynamic therapy. ACS Appl Mater Interfaces. 2020;12:1988–96.
164. Mederos N, Friedlaender A, Peters S, Addeo A. Gender-specific aspects of epidemiology, molecular genetics and outcome: lung cancer. ESMO Open. 2020;5: e000796.
165. Maconachie R, Mercer T, Navani N, McVeigh G. Lung cancer: diagnosis and management: summary of updated NICE guidance. BMJ. 2019;364: l1049.
166. Hurmuz P, Cengiz M, Ozyigit G, Akkas EA, Yuce D, Yilmaz MT, Yildiz D, Zorlu F, Akyol F. Stereotactic body radiotherapy in patients with early-stage non-small cell lung cancer: does beam-on time matter? Japanese J Clin Oncol. 2020;50:1182–7.
167. Faehling M, Witte H, Sebastian M, Ulmer M, Sätzler R, Steinestel K, Brückl WM, Evers G, Büschenfelde CM, Bleckmann A. Real-world multicentre analysis of neoadjuvant immunotherapy and chemotherapy in

localized or oligometastatic non-small cell lung cancer (KOMPASSneoOP). Ther Adv Med Oncol. 2022;14:17588359221085332.
168. Lu X, Liu S, Han M, Yang X, Sun K, Wang H, Mu H, Du Y, Wang A, Ni L, Zhang C. Afatinib-loaded immunoliposomes functionalized with cetuximab: A novel strategy targeting the epidermal growth factor receptor for treatment of non-small-cell lung cancer. Int J Pharm. 2019;560:126–35.
169. Gao M, Su H, Lin G, Li S, Yu X, Qin A, Zhao Z, Zhang Z, Tang BZ. Targeted imaging of EGFR overexpressed cancer cells by brightly fluorescent nanoparticles conjugated with cetuximab. Nanoscale. 2016;8:15027–32.
170. Su H, Deng Z, Liu Y, Zhao Y, Liu H, Zhao Z, Tang BZ. A brightly red emissive AIEgen and its antibody conjugated nanoparticles for cancer cell targeting imaging. Mater Chem Front. 2022;6:1317–23.
171. Wang C, Zhao X, Jiang H, Wang J, Zhong W, Xue K, Zhu C. Transporting mitochondrion-targeting photosensitizers into cancer cells by low-density lipoproteins for fluorescence-feedback photodynamic therapy. Nanoscale. 2021;13:1195–205.
172. Arnesano F, Nardella MI, Natile G. Platinum drugs, copper transporters and copper chelators. Coord Chem Rev. 2018;374:254–60.
173. Shim MK, Moon Y, Yang S, Kim J, Cho H, Lim S, Yoon HY, Seong JK, Kim K. Cancer-specific drug-drug nanoparticles of pro-apoptotic and cathepsin B-cleavable peptide-conjugated doxorubicin for drug-resistant cancer therapy. Biomaterials. 2020;261: 120347.
174. Su Y, Lin H, Tu Y, Wang MM, Zhang GD, Yang J, Liu HK, Su Z. Fighting metallodrug resistance through alteration of drug metabolism and blockage of autophagic flux by mitochondria-targeting AIEgens. Chem Sci. 2022;13:1428–39.
175. Deng J, Yang M, Li C, Liu G, Sun Q, Luo X, Wu F. Single molecular-based nanoparticles with aggregation-induced emission characteristics for fluorescence imaging and efficient cancer phototherapy. Dyes Pigm. 2021;187: 109130.
176. Zheng Y, Lu H, Jiang Z, Guan Y, Zou J, Wang X, Cheng R, Gao H. Low-power white light triggered AIE polymer nanoparticles with high ROS quantum yield for mitochondria-targeted and image-guided photodynamic therapy. J Mater Chem B. 2017;5:6277–81.
177. Xiao YF, Chen WC, Chen JX, Lu G, Tian S, Cui X, Zhang Z, Chen H, Wan Y, Li S, Lee CS. Amplifying free radical generation of AIE photosensitizer with small singlet–triplet splitting for hypoxia-overcoming photodynamic therapy. ACS Appl Mater Interfaces. 2022;14:5112–21.
178. Cao S, Xia Y, Shao J, Guo B, Dong Y, Pijpers IAB, Zhong Z, Meng F, Abdelmohsen LKEA, Williams DS, van Hest JCM. Biodegradable polymersomes with structure inherent fluorescence and targeting capacity for enhanced photo-dynamic therapy. Angew Chem Int Ed. 2021;60:17629–37.
179. Siegel RL, Miller KD, Fuchs HE, Jemal A. Cancer statistics, 2022. CaCancer J Clins. 2022;72:7–33.
180. Yu J, Mu Q, Fung M, Xu X, Zhu L, Ho RJY. Challenges and opportunities in metastatic breast cancer treatments: Nano-drug combinations delivered preferentially to metastatic cells may enhance therapeutic response. Pharmacol Ther. 2022;236: 108108.
181. Wang Y, Yu Y, Chen K, Fu T, Yao H. Locoregional surgery of the primary tumor in stage IV breast cancer patients. J Clin Oncol. 2017;35:566–566.
182. Poleszczuk J, Luddy K, Chen L, Lee JK, Harrison LB, Czerniecki BJ, Soliman H, Enderling H. Neoadjuvant radiotherapy of early-stage breast cancer and long-term disease-free survival. Breast Cancer Res. 2017;19:75.
183. Barinoff J, Schmidt M, Schneeweiss A, Schoenegg W, Thill M, Keitel S, Lattrich CR, Hinke A, Kutscheidt A, Jackisch C. Primary metastatic breast cancer in the era of targeted therapy—prognostic impact and the role of breast tumour surgery. Eur J Cancer. 2017;83:116–24.
184. Jyotsana N, Zhang Z, Himmel Lauren E, Yu F, King Michael R. Minimal dosing of leukocyte targeting TRAIL decreases triple-negative breast cancer metastasis following tumor resection. Sci Adv. 2019;5:4197.
185. Rios Garcia M, Steinbauer B, Srivastava K, Singhal M, Mattijssen F, Maida A, Christian S, Hess Stumpp H, Augustin HG, Müller Decker K, et al. Acetyl-CoA carboxylase 1-dependent protein acetylation controls breast cancer metastasis and recurrence. Cell Metab. 2017;26:842-855.e845.
186. Jiang R, Dai J, Dong X, Wang Q, Meng Z, Guo J, Yu Y, Wang S, Xia F, Zhao Z, et al. Improving image-guided surgical and immunological tumor treatment efficacy by photothermal and photodynamic therapies based on a multifunctional NIR AIEgen. Adv Mater. 2021;33:2101158.
187. Su Y, Tu Y, Lin H, Wang MM, Zhang GD, Yang J, Liu HK, Su Z. Mitochondria-targeted Pt(IV) prodrugs conjugated with an aggregation-induced emission luminogen against breast cancer cells by dual modulation of apoptosis and autophagy inhibition. J Inorg Biochem. 2022;226: 111653.
188. Liu L, Wang X, Wang LJ, Guo L, Li Y, Bai B, Fu F, Lu H, Zhao X. One-for-all phototheranostic agent based on aggregation-induced emission characteristics for multimodal imaging-guided synergistic photodynamic/photothermal cancer therapy. ACS Appl Mater Interfaces. 2021;13:19668–78.
189. Wang Y, Gong N, Li Y, Lu Q, Wang X, Li J. Atomic-level nanorings (A-NRs) therapeutic agent for photoacoustic imaging and photothermal/photodynamic therapy of cancer. J Am Chem Soc. 2020;142:1735–9.
190. Zhao X, Long S, Li M, Cao J, Li Y, Guo L, Sun W, Du J, Fan J, Peng X. Oxygen-dependent regulation of excited-state deactivation process of rational photosensitizer for smart phototherapy. J Am Chem Soc. 2020;142:1510–7.
191. Shao W, Yang C, Li F, Wu J, Wang N, Ding Q, Gao J, Ling D. Molecular design of conjugated small molecule nanoparticles for synergistically enhanced PTT/PDT. Nanomicro Lett. 2020;12:147.
192. Zhang Z, Xu W, Kang M, Wen H, Guo H, Zhang P, Xi L, Li K, Wang L, Wang D, Tang BZ. An all-round athlete on the track of phototheranostics: subtly regulating the balance between radiative and nonradiative decays for multimodal imaging-guided synergistic therapy. Adv Mater. 2020;32:2003210.
193. Zhang L, Jing D, Jiang N, Rojalin T, Baehr CM, Zhang D, Xiao W, Wu Y, Cong Z, Li JJ, et al. Transformable peptide nanoparticles arrest HER2 signalling and cause cancer cell death in vivo. Nat Nanotechnol. 2020;15:145–53.
194. Liao Y, Wang R, Wang S, Xie Y, Chen H, Huang R, Shao L, Zhu Q, Liu Y. Highly efficient multifunctional organic photosensitizer with aggregation-induced emission for *in vivo* bioimaging and photodynamic therapy. ACS Appl Mater Interfaces. 2021;13:54783–93.
195. Huang L, Qing D, Zhao S, Wu X, Yang K, Ren X, Zheng X, Lan M, Ye J, Zeng L, Niu G. Acceptor-donor-acceptor structured deep-red AIE photosensitizer: lysosome-specific targeting, in vivo long-term imaging, and effective photodynamic therapy. Chem Eng J. 2022;430: 132638.
196. Siegel RL, Miller KD, Fuchs HE, Jemal A. Cancer statistics, 2021. CA Cancer J Clins. 2021;71:7–33.
197. Siegel RL, Miller KD, Fedewa SA, Ahnen DJ, Meester RGS, Barzi A, Jemal A. Colorectal cancer statistics, 2017. CA Cancer J Clins. 2017;67:177–93.
198. Montminy EM, Zhou M, Maniscalco L, Abualkhair W, Kim MK, Siegel RL, Wu XC, Itzkowitz SH, Karlitz JJ. Contributions of adenocarcinoma and carcinoid tumors to early-onset colorectal cancer incidence rates in the united states. Ann Intern Med. 2020;174:157–66.
199. Schreuders EH, Ruco A, Rabeneck L, Schoen RE, Sung JJY, Young GP, Kuipers EJ. Colorectal cancer screening: a global overview of existing programmes. Gut. 2015;64:1637.
200. Nelson H, Petrelli N, Carlin A, Couture J, Fleshman J, Guillem J, Miedema B, Ota D, Sargent D. Guidelines 2000 for colon and rectal cancer surgery. JNCI J Natl Cancer Inst. 2001;93:583–96.
201. Charlton ME, Jiang D, Lin C, Stitzenberg KB, Pendergast JF, Chrischilles EA, Wallace RB. Factors associated with use of preoperative chemoradiotherapy for rectal cancer. J Clin Oncol. 2011;29:e14079–e14079.
202. Shen J, Tao K, Gu P, Gui C, Wang D, Tan Z, Wang L, Wang Z, Qin A, Tang BZ, Bao S. Aggregation-induced emission luminogen for specific identification of malignant tumour in vivo. Sci China Chem. 2020;63:393–7.
203. He H, Liu L, Liang R, Zhou H, Pan H, Zhang S, Cai L. Tumor-targeted nanoplatform for in situ oxygenation-boosted immunogenic phototherapy of colorectal cancer. Acta Biomater. 2020;104:188–97.
204. Yang H, Zhuang J, Li N, Li Y, Zhu S, Hao J, Xin J, Zhao N. Efficient near-infrared photosensitizer with aggregation-induced emission characteristics for mitochondria-targeted and image-guided photodynamic cancer therapy. Mater Chem Front. 2020;4:2064–71.
205. Gao S, Yu S, Zhang Y, Wu A, Zhang S, Wei G, Wang H, Xiao Z, Lu W. Molecular engineering of near-Infrared-II photosensitizers with steric-hindrance effect for image-guided cancer photodynamic therapy. Adv Funct Mater. 2021;31:2008356.

206. Min X, Yi F, Han XL, Li M, Gao Q, Liang X, Chen Z, Sun Y, Liu Y. Targeted photodynamic therapy using a water-soluble aggregation-induced emission photosensitizer activated by an acidic tumor microenvironment. Chem Eng J. 2022;432: 134327.
207. Zhang YH, Li X, Huang L, Kim HS, An J, Lan M, Cao QY, Kim JS. AIE based GSH activatable photosensitizer for imaging-guided photodynamic therapy. Chem Commun. 2020;56:10317–20.
208. Swami U, McFarland TR, Nussenzveig R, Agarwal N. Advanced prostate cancer: treatment advances and future directions. Trends Cancer. 2020;6:702–15.
209. Siegel RL, Miller KD, Fuchs HE, Jemal A. Cancer statistics, 2021. CA Cancer J Clins. 2021;71:359–359.
210. Huang J, Lin B, Li B. Anti-androgen receptor therapies in prostate cancer: a brief update and perspective. Front Oncol. 2022;12:865350.
211. Kretschmer A, Tilki D. Biomarkers in prostate cancer-current clinical utility and future perspectives. Crit Rev Oncol Hematol. 2017;120:180–93.
212. Wang X, Ramamurthy G, Shirke AA, Walker E, Mangadlao J, Wang Z, Wang Y, Shan L, Schluchter MD, Dong Z, et al. Photodynamic therapy is an effective adjuvant therapy for image-guided surgery in prostate cancer. Cancer Res. 2020;80:156–62.
213. Jayaram DT, Ramos Romero S, Shankar BH, Garrido C, Rubio N, Sanchez-Cid L, Gómez SB, Blanco J, Ramaiah D. In vitro and in vivo demonstration of photodynamic activity and cytoplasm imaging through TPE nanoparticles. ACS Chem Biol. 2016;11:104–12.
214. Ghosh S, Gul AR, Xu P, Lee SY, Rafique R, Kim YH, Park TJ. Target delivery of photo-triggered nanocarrier for externally activated chemo-photodynamic therapy of prostate cancer. Mater Today Chem. 2022;23: 100688.
215. Tan H, Hou N, Liu Y, Liu B, Cao W, Zheng D, Li W, Liu Y, Xu B, Wang Z, Cui D. CD133 antibody targeted delivery of gold nanostars loading IR820 and docetaxel for multimodal imaging and near-infrared photodynamic/photothermal/chemotherapy against castration resistant prostate cancer. Nanomedicine. 2020;27: 102192.
216. Bouffard E, Mauriello Jimenez C, El Cheikh K, Maynadier M, Basile I, Raehm L, Nguyen C, Gary Bobo M, Garcia M, Durand JO, Morère A. Efficient photodynamic therapy of prostate cancer cells through an improved targeting of the cation-independent mannose 6-phosphate receptor. Int J Mol Sci. 2019;20:2809.
217. Overchuk M, Damen MPF, Harmatys KM, Pomper MG, Chen J, Zheng G. Long-circulating prostate-specific membrane antigen-targeted NIR phototheranostic agent. Photochem Photobiol. 2020;96:718–24.
218. Liu Q, Huang J, He L, Yang X, Yuan L, Cheng D. Molecular fluorescent probes for liver tumor imaging. Chem Asian J. 2022;17: e202200091.
219. Bray F, Ferlay J, Soerjomataram I, Siegel RL, Torre LA, Jemal A. Global cancer statistics 2018: GLOBOCAN estimates of incidence and mortality worldwide for 36 cancers in 185 countries. CA Cancer J Clins. 2018;68:394–424.
220. EASL clinical practice guidelines. management of hepatocellular carcinoma. J Hepatol. 2018;69:182–236.
221. Patel K, Lamm R, Altshuler P, Dang H, Shah AP. Hepatocellular carcinoma-the influence of immunoanatomy and the role of immunotherapy. Int J Mol Sci. 2020;21:6757.
222. Tsilimigras DI, Bagante F, Sahara K, Moris D, Hyer JM, Wu L, Ratti F, Marques HP, Soubrane O, Paredes AZ, et al. Prognosis after resection of barcelona clinic liver cancer (BCLC) stage 0, A, and B hepatocellular carcinoma: a comprehensive assessment of the current BCLC classification. Ann Surg Oncol. 2019;26:3693–700.
223. Verslype C, Rosmorduc O, Rougier P. Hepatocellular carcinoma: ESMO–ESDO clinical practice guidelines for diagnosis, treatment and follow-up. Ann Oncol. 2012;23:vii41–8.
224. Bruix J, Sherman M. Management of hepatocellular carcinoma: an update. Hepatology. 2011;53:1020–2.
225. Bruix J, Reig M, Sherman M. Evidence-based diagnosis, staging, and treatment of patients with hepatocellular carcinoma. Gastroenterology. 2016;150:835–53.
226. Koda M, Murawaki Y, Hirooka Y, Kitamoto M, Ono M, Sakaeda H, Joko K, Sato S, Tamaki K, Yamasaki T, et al. Complications of radiofrequency ablation for hepatocellular carcinoma in a multicenter study: an analysis of 16 346 treated nodules in 13 283 patients. Hepatol Res. 2012;42:1058–64.
227. Teng M, Chen Y, Xie Y, Li Z, Wan Q, Wang Z, Yang J. Bright near-infrared aggregation-induced emission dots for long-term bioimaging in vitro/vivo. Dyes Pigm. 2021;195: 109679.
228. Xia Q, Chen Z, Zhou Y, Liu R. Near-infrared organic fluorescent nanoparticles for long-term monitoring and photodynamic therapy of cancer. J Nanotheranostics. 2019;3:156–65.
229. Dineshkumar S, Raj A, Srivastava A, Mukherjee S, Pasha SS, Kachwal V, Fageria L, Chowdhury R, Laskar IR. Facile incorporation of "aggregation-induced emission"-active conjugated polymer into mesoporous silica hollow nanospheres: synthesis, characterization, photophysical studies, and application in bioimaging. ACS Appl Mater Inter. 2019;11:31270–82.
230. Gao Y, Zheng QC, Xu S, Yuan Y, Cheng X, Jiang S, Kenry YuQ, Song Z, Liu B, Li M. Theranostic nanodots with aggregation-induced emission characteristic for targeted and image-guided photodynamic therapy of hepatocellular carcinoma. Theranostics. 2019;9:1264–79.
231. Zhao D, Han HH, Zhu L, Xu FZ, Ma XY, Li J, James TD, Zang Y, He XP, Wang C. Long-wavelength AIE-based fluorescent probes for mitochondria-targeted imaging and photodynamic therapy of hepatoma cells. ACS Appl Bio Mater. 2021;4:7016–24.
232. Ding K, Wang L, Zhu J, He D, Huang Y, Zhang W, Wang Z, Qin A, Hou J, Tang BZ. Photo-enhanced chemotherapy performance in bladder cancer treatment via albumin coated AIE aggregates. ACS Nano. 2022;16:7535–46.
233. Duo Y, Zhu D, Sun X, Suo M, Zheng Z, Jiang W, Tang BZ. Patient-derived microvesicles/AIE luminogen hybrid system for personalized sonodynamic cancer therapy in patient-derived xenograft models. Biomaterials. 2021;272: 120755.
234. Sun X, Zebibula A, Dong X, Li G, Zhang G, Zhang D, Qian J, He S. Targeted and imaging-guided in vivo photodynamic therapy for tumors using dual-function, aggregation-induced emission nanoparticles. Nano Res. 2018;11:2756–70.
235. Sun X, Zebibula A, Dong X, Zhang G, Zhang D, Qian J, He S. Aggregation-induced emission nanoparticles encapsulated with PEGylated nano graphene oxide and their applications in two-photon fluorescence bioimaging and photodynamic therapy in vitro and *in vivo*. ACS Appl Mater Interfaces. 2018;10:25037–46.
236. Hao J, Yin H, Lu W, Zhuang J, Chen M, Gao J, Zhu G, Cao W, Kan Y, Lu Y, Guo H. Modulating endogenous oxygen consumption enhanced AIEgens-mediated photodynamic therapy against advanced bladder tumor. Part Part Syst Charact. 2021;38:2100048.
237. Lauterio A, De Carlis R, Centonze L, Buscemi V, Incarbone N, Vella I, De Carlis L. Current surgical management of peri-hilar and intra-hepatic cholangiocarcinoma. Cancers. 2021;13:3657.
238. Pear S, Bachini M, Gardett I, Lindsey S, Delcorso Ellmann T, Abdel WR. Barriers for clinical trial enrollment in cholangiocarcinoma patients. J Clin Oncol. 2022;40:407–407.
239. Li H, Chen L, Zhu GY, Yao X, Dong R, Guo J-H. Interventional treatment for cholangiocarcinoma. Front Oncol. 2021;11:671327.
240. Bai M, Fu W, Su G, Cao J, Gao L, Huang C, Ma H, Zhang J, Yue P, Bai B, et al. The role of extracellular vesicles in cholangiocarcinoma. Cancer Cell Int. 2020;20:435.
241. Samatiwat P, Prawan A, Senggunprai L, Kukongviriyapan V. Repression of Nrf2 enhances antitumor effect of 5-fluorouracil and gemcitabine on cholangiocarcinoma cells. Naunyn Schmiedebergs Arch Pharmacol. 2015;388:601–12.
242. Rahnemai Azar AA, Weisbrod AB, Dillhoff M, Schmidt C, Pawlik TM. Intrahepatic cholangiocarcinoma: current management and emerging therapies. Expert Rev Gastroenterol Hepatol. 2017;11:439–49.
243. Massironi S, Pilla L, Elvevi A, Longarini R, Rossi RE, Bidoli P, Invernizzi P. New and emerging systemic therapeutic options for advanced cholangiocarcinoma. Cells. 2020;9:688.
244. Rumalla A, Baron TH, Wang KK, Gores GJ, Stadheim LM, de Groen PC. Endoscopic application of photodynamic therapy for cholangiocarcinoma. Gastrointest Endosc. 2001;53:500–4.
245. Kumta NA, DeRoche K, Kahaleh M. Temoporfin photodynamic therapy in advanced hilar ductal carcinoma: a promising endoscopic modality. Hepatology. 2015;62:1342–3.
246. Kahaleh M. Photodynamic therapy in cholangiocarcinoma. J Natl Compr Canc Netw. 2012;10:S44–7.

247. Lamarca A, Edeline J, McNamara MG, Hubner RA, Nagino M, Bridgewater J, Primrose J, Valle JW. Current standards and future perspectives in adjuvant treatment for biliary tract cancers. Cancer Treat Rev. 2020;84:101936.
248. Li M, Gao Y, Yuan Y, Wu Y, Song Z, Tang BZ, Liu B, Zheng QC. One-step formulation of targeted aggregation-induced emission dots for image-guided photodynamic therapy of cholangiocarcinoma. ACS Nano. 2017;11:3922–32.
249. Zhou T, Zhu J, Shang D, Chai C, Li Y, Sun H, Li Y, Gao M, Li M. Mitochondria-anchoring and AIE-active photosensitizer for self-monitored cholangiocarcinoma therapy. Mater Chem Front. 2020;4:3201–8.

Publisher's Note